Observations of 1,2-dichloroethane from the AGAGE and NOAA networks and derived global and regional emissions

Joseph R. Pitt[1]*, Dominique Rust[1]*, Anita Ganesan[2], Luke M. Western[3], Martin K. Vollmer[4], Jens Mühle[5], Tobias Bühlmann[6], Christina M. Harth[5], Stephen A. Montzka[7], Brad D. Hall[7], Isaac J. Vimont[7], Alistair J. Manning[1,8], Alison L. Redington[8], Stephan Henne[4], Daniela B. Melo[4], Saurabh Annadate[9,10,18], Lionel Constantin[4], Brendan M. Murphy[1], Matthew Rigby[1], Dickon Young[1], Simon O'Doherty[1], Angelina Wenger[1], Chris R. Lunder[11], Ove Hermansen[11], Thomas Wagenhäuser[12], Andreas Engel[12], Jgor Arduini[9,10], Michela Maione[9,10], Jaegeun Yun[13], Blagoj Mitrevski[14], Paul B. Krummel[14], Paul J. Fraser[14], Jooil Kim[5], Ray H. J. Wang[15], Tae Siek Rhee[16], Peter K. Salameh[17], T. Gerard Spain[18], Stefan Reimann[4], Ronald G. Prinn[3], Ray F. Weiss[5], and Kieran M. Stanley[1]

[1]Atmospheric Chemistry Research Group, School of Chemistry, University of Bristol, Bristol, United Kingdom
[2]School of Geographical Sciences, University of Bristol, Bristol, United Kingdom
[3]Center for Sustainability Science and Strategy, Massachusetts Institute of Technology, Cambridge, MA, USA
[4]Laboratory for Air Pollution/Environmental Technology, Empa, Swiss Federal Laboratories for Materials Science and Technology, Dübendorf, Switzerland
[5]Scripps Institution of Oceanography, University of California San Diego, La Jolla, CA, USA
[6]Laboratory for Gas Analysis, METAS, Federal Institute of Metrology, Bern-Wabern, Switzerland
[7]NOAA Global Monitoring Laboratory, Boulder, CO, USA
[8]Met Office Hadley Centre, Exeter, United Kingdom
[9]Department of Pure and Applied Sciences, University of Urbino, Urbino, Italy
[10]Institute of Atmospheric Sciences and Climate, Italian National Research Council, Bologna, Italy
[11]NILU, Kjeller, Norway
[12]Institute for Atmospheric and Environmental Sciences, Goethe University, Frankfurt am Main, Germany
[13]School of Earth System Sciences, Kyungpook National University, Daegu, South Korea
[14]CSIRO Environment, Aspendale, Victoria, Australia
[15]School of Earth and Atmospheric Sciences, Georgia Institute of Technology, Atlanta, GA, USA
[16]Korea Polar Research Institute, KIOST, Incheon, South Korea
[17]GC Soft Inc., Carlsbad, CA, USA
[18]School of Natural Sciences, University of Galway, Galway, Ireland
*These authors contributed equally to this work.

Correspondence to: Joseph R. Pitt (joseph.pitt@bristol.ac.uk) and Dominique Rust (dominique.rust@bristol.ac.uk)

Abstract. For the first time, we present long-term, ongoing atmospheric measurements of 1,2-dichloroethane (DCE, CH_2ClCH_2Cl) from the Advanced Global Atmospheric Gases Experiment (AGAGE) and National Oceanic and Atmospheric Administration (NOAA) global monitoring networks. DCE is an industrially produced, very short-lived chlorinated substance (Cl-VSLS) that has the potential to contribute chlorine to the stratosphere and cause ozone depletion. Compared to other Cl-VSLS, DCE is produced in higher volumes for its primary use as a feedstock in polyvinyl chloride (PVC) manufacture. This production has sustained annual mean mole fractions at the Earth's surface of between 5 and 10 ppt during 2017–2023, making it the third most abundant Cl-VSLS after dichloromethane and chloroform. In this study we estimate mean global emissions for 2017–2023 of 453 ± 185 Gg yr^{-1} using the AGAGE observations, and 525 ± 209 Gg yr^{-1} using the NOAA observations.

We also use AGAGE measurements to estimate regional emissions for northwest Europe (2.06 [1.31, 2.65] Gg yr^{-1}) and California (0.23 [0, 0.37] Gg yr^{-1}), two domains with sufficient observational coverage to enable this approach. Our global emissions estimates are consistent (within uncertainties) with the only previously published estimate by Hossaini et al. (2024), whereas our regional emission estimates are at least an order of magnitude smaller than those in that study. This suggests global total emissions may be well constrained, but their spatial distribution remains uncertain.

1 Introduction

Chlorinated very short-lived substances (Cl-VSLS) are increasingly being studied to better understand their impact on stratospheric ozone depletion through their contribution to stratospheric chlorine levels. Although the ozone depletion potentials (ODPs) of Cl-VSLS are low compared to many long-lived ozone depleting substances (ODSs) controlled by the Montreal Protocol on Substances that Deplete the Ozone Layer, in several cases they are not negligible (Burkholder and Hodnebrog et al., 2022; Hossaini et al., 2024; UNEP, 2022), and they vary depending on the season and location of emissions. Unlike long-lived ODSs, the production and consumption of Cl-VSLS is not controlled under the Montreal Protocol, even though increasing atmospheric abundances of Cl-VSLS are partially offsetting decreases in ODS abundances and delaying the recovery of the stratospheric ozone layer (Bednarz et al., 2022, 2023; Chipperfield and Santee et al., 2022; Daniel and Reimann et al., 2022; Hossaini et al., 2019; Laube and Tegtmeier et al., 2022; Oram et al., 2017; Villamayor et al., 2023). Due to their short atmospheric lifetimes (typically less than 6 months), the total radiative forcing of Cl-VSLS is small. However, they may nonetheless have some impact on the global radiative balance (Braesicke and Neu et al., 2018; Hossaini et al., 2015). The Advanced Global Atmospheric Gases Experiment (AGAGE) and the National Oceanic and Atmospheric Administration (NOAA) measurement networks monitor the atmospheric abundance of several Cl-VSLS with high production volumes such as dichloromethane (methylene chloride, DCM, CH_2Cl_2), tetrachloroethene (perchloroethylene, PCE, CCl_2CCl_2), and trichloromethane (chloroform, CFM, $CHCl_3$). The atmospheric abundance of DCM has more than doubled since the year 2000 (Laube and Tegtmeier et al., 2022).

Currently, the chlorinated substance 1,2-dichloroethane (ethylene dichloride, DCE, DCA, CH_2ClCH_2Cl, CAS No. 107-06-2) is produced in markedly higher volumes than other Cl-VSLS (UNEP, 2022). The total global production in 2020 was estimated to be larger than 50,000 Gg (Hossaini et al., 2024; MCgroup, 2023; Statista, 2023; TEAP, 2024; UNEP, 2018, 2022). The largest production centres lie in East Asia, the United States (predominantly Louisiana, Texas and Kentucky (EPA, 2025a)), and Europe (UNEP, 2022). These are also the dominant regions for DCE consumption (UNEP, 2022). The main use of DCE (95–99 %; CEH, 2025; ECHA, 2012; Hossaini et al., 2024; TEAP, 2024; UNEP, 2002, 2018, 2022) is as a feedstock in the industrial manufacture of vinyl chloride monomer (VCM), which is polymerised to polyvinyl chloride (PVC), one of the most widely produced plastic polymers (Hossaini et al., 2024; TEAP, 2024; UNEP, 2022). Other minor feedstock uses include the production of trichloroethene (trichloroethylene, TCE, CCl_2CHCl), PCE, and ethylene amines, and DCE is also used as a solvent, although many of these solvent uses are poorly documented (Arcoya et al., 1980b, a; Ayres and Ayres, 1997; EPA,

2020a; Hossaini et al., 2024; Sutherland et al., 2011; Takahashi et al., 2024; TEAP, 2024; UNEP, 2018, 2022; Wu and An, 2024). Due to the recognised toxicity of DCE, its use is subject to regulatory control in several countries and regions, including the United States and the European Union (ECHA, 2022; EPA, 2020b, 2024, 2026; Sherwood, 2018; UNEP, 2022).

The only known source of DCE to the atmosphere is due to anthropogenic activities (Engel and Rigby et al., 2018; Hossaini et al., 2015). Emissions are thought to be via fugitive losses from feedstock use, including production, consumption, shipping, and storage (Hossaini et al., 2024; UNEP, 2022). Emissions also occur from directly emissive applications such as its use as a solvent (Hossaini et al., 2024; UNEP, 2022). A recent study by Hossaini et al. (2024) published the first emission estimates of DCE based on a statistical bottom-up methodology, informed by atmospheric measurements taken during three aircraft campaigns and surface measurements from Southeast Asia. Hossaini et al. (2024) suggested that global DCE emissions increased by 45% over the last two decades (from 349 Gg in 2002 to 505 Gg in 2020; Hossaini et al., 2024). However, they point out the uncertainties in the magnitude of direct DCE emissions, since there are no reporting requirements for the production or consumption of DCE for solvent use.

Once emitted, DCE has a mean tropospheric lifetime of approximately 83 days (Hossaini et al., 2024). However, the local atmospheric lifetimes of DCE and other Cl-VSLS are dependent on the time of year and regional atmospheric conditions (Hodnebrog et al., 2020), leading to pronounced spatiotemporal variability in their tropospheric abundances (Laube et al., 2008; Law and Sturges et al., 2006). Therefore, the fraction of emitted DCE and its atmospheric degradation products (Hossaini et al., 2024) that can reach the stratosphere depends on emission locations relative to the corresponding loss regions and vertical transport mechanisms (Brioude et al., 2010; Claxton et al., 2019; Liang et al., 2025; Pan et al., 2024; Pisso et al., 2010). Unexpectedly enhanced levels of Cl-VSLS were observed in the upper troposphere up to the lower stratosphere Asian Summer Monsoon outflow, suggesting that this is a region from which emissions can be transported to the stratosphere particularly efficiently (Adcock et al., 2020; Jesswein et al., 2025; Lauther et al., 2022; Pan et al., 2024). Given the shorter lifetime of DCE compared to the other Cl-VSLS considered here, the efficiency with which emissions reach the stratosphere is more sensitive to location (Claxton et al., 2019). Hossaini et al. (2024) estimate an input of 12.9 ppt (parts per trillion, pmol mol^{-1}) of stratospheric chlorine due to DCE in 2020. This can be compared to the contribution to total stratospheric chlorine from Cl-VSLS of ~130 (100–160) ppt in 2020 (Bednarz et al., 2022; Laube and Tegtmeier et al., 2022). The regionally varying ODP of DCE was calculated at 0.0029–0.0119 (Claxton et al., 2019). Its current contribution to direct stratospheric ozone depletion was estimated to be comparatively small (less than 1 % as an annual average in 2020) (Hossaini et al., 2024), but this contribution is associated with high uncertainty due to its dependence on DCE emission location and time (Daniel and Reimann et al., 2022; Hossaini et al., 2024; Laube and Tegtmeier et al., 2022). Hence, additional monitoring for characterising emissions of DCE and other VSLS on regional scales could help to constrain their contributions to stratospheric chlorine content.

Periodic measurements of the tropospheric abundance of DCE were conducted in the last two decades during aircraft campaigns (Roozitalab et al., 2024; Thompson et al., 2022; Wofsy, 2011; Wofsy et al., 2017, 2021) over both hemispheres, principally covering the Pacific, the Arctic, the Southern, and the Atlantic Oceans, Alaska, and parts of the Antarctic. These campaigns provide data for all seasons. During these campaigns, boundary layer mole fractions were found in the range of 10–

20 ppt in the Northern Hemisphere, and at approximately 2 ppt for the Southern Hemisphere (Engel and Rigby et al., 2018; Hossaini et al., 2019, 2024; Laube and Tegtmeier et al., 2022; Roozitalab et al., 2024). In addition, in the last two decades, aircraft (Crawford et al., 2021; NASA, 2024; Oram et al., 2017; Pan et al., 2024; Simpson et al., 2020) and short-term (a few months) to medium-term (up to three years) ground-based measurement campaigns were conducted that principally covered land regions (Crawford et al., 2021; Logue et al., 2010; Lyu et al., 2020; Mao et al., 2009; NASA, 2024; Oram et al., 2017; Simpson et al., 2020; Yang et al., 2016; Zhang et al., 2014). These campaigns captured air masses that were regionally or locally influenced by urban and/or industrial sources. Mole fractions were particularly reported from regions of China, other Asian countries, and the USA. The measured mole fractions exhibit a large spatiotemporal variability, reaching magnitudes of a couple of tens to a couple of hundreds of ppt; some studies even reported pollution events at the thousands of ppt level (Barletta et al., 2009; Simpson et al., 2020; Xu et al., 2023). In all studies, the reported mean mole fractions of DCE and/or the relative contribution of DCE to the sum of chlorine (Oram et al., 2017) were among the highest of the respectively analysed VSLS, after DCM and CFM.

Here we present, for the first time, ongoing surface-based measurements of DCE from the AGAGE (AGAGE, 2025; Prinn et al., 2018) and NOAA (NOAA, 2025) global measurement networks. The observations at a total of 20 sampling locations across the globe cover the years 2017–2023. With measurements of archived air samples from three sites, we extend the record back to 1995. Using a top-down approach based on these long-term atmospheric observations, we estimate global emissions as well as regional emissions for northwest (NW) Europe and California (two regions for which we have sufficient measurement coverage to enable this approach). Our results help to better constrain the environmental impact of DCE as one of the most highly emitted industrially produced VSLS.

2 Materials and methods

2.1 Measurement sites

This study presents DCE measurements from the AGAGE (AGAGE, 2025; Prinn et al., 2018) and NOAA (NOAA, 2025) global measurement networks. These networks sample air at long-term measurement sites that are sensitive to emissions from different global regions and capture global background mole fractions in well-mixed air masses, as well as, in some cases, regional pollution events. The sites and their associated three-letter abbreviations are shown on a map in Fig. 1 and listed in Appendix B. Sites are referred to throughout by their three-letter abbreviations for ease of reference against Fig. 1. In situ measurements made within AGAGE are reported from 11 field sites. Measurements from the station at Gosan (South Korea), have been excluded from this study due to data issues (see Sect. 2.2).

Measurements of DCE from paired flask samples collected by the NOAA Global Monitoring Laboratory (GML) are reported from 16 sites. Samples were collected approximately weekly. The main change in the NOAA sampling network through this period at these sites occurred at the MLO site in November 2022, when the eruption of the Mauna Loa volcano terminated power and road access to the site. Prior to that date, measurements at MLO were obtained from paired stainless-steel flasks

collected manually between 10:00 and 12:00 local time. After that date, results were from paired glass flasks collected automatically at 05:00 local time. The two flask collection methods were used side-by-side at MLO from July 2021 to November 2022. During this time, the difference in monthly mean DCE mole fraction calculated using glass flask samples instead of stainless-steel flask samples was less than 0.5 % on average.

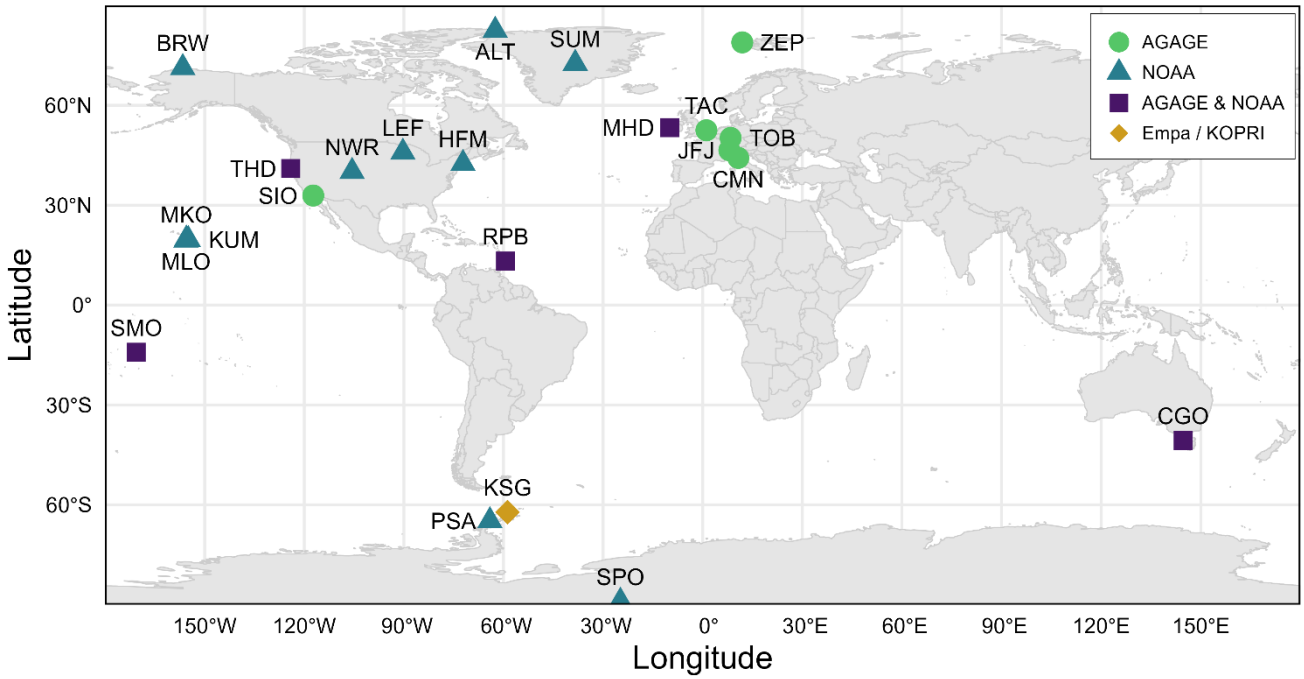

Figure 1: In situ and flask measurements sites for 1,2-dichloroethane (DCE). Green circles: AGAGE. Cyan triangles: NOAA. Dark purple squares: sites in both the AGAGE and NOAA networks. Golden diamond: Empa/KOPRI flask measurements. Alert, Canada (ALT); Zeppelin, Svalbard, Norway (ZEP); Summit, Greenland (SUM); Barrow, Alaska, USA (BRW); Mace Head, Ireland (MHD); Tacolneston, UK (TAC); Taunus, Germany (TOB); Jungfraujoch, Switzerland (JFJ); Park Falls, Wisconsin, USA (LEF); Monte Cimone, Italy (CMN); Harvard Forest, Massachusetts, USA (HFM); Trinidad Head, California, USA (THD); Niwot Ridge, Colorado, USA (NWR); Scripps Institution of Oceanography, California, USA (SIO); Mauna Kea, Hawaii, USA (MKO); Cape Kumukahi, Hawaii, USA (KUM); Mauna Loa, Hawaii, USA (MLO); Ragged Point, Barbados (RPB); Cape Matatula, American Samoa (SMO); Kennaook/Cape Grim, Tasmania, Australia (CGO); King Sejong Station, Antarctica (KSG); Palmer Station, Antarctica (PSA); South Pole, Antarctica (SPO).

Measurements of flask samples, collected weekly at the King Sejong Station (KSG, Antarctica) (Vollmer et al., 2011, 2018) from 2016–2024, complement the AGAGE measurement record. These flasks were collected by the Korea Polar Research Institute (KOPRI) and analysed by the Swiss Federal Laboratories for Materials Science and Technology (Empa). In addition, a set of 9 sub-samples from cryogenically filled samples of the Cape Grim Air Archive (CGAA, Tasmania, Australia) (Langenfelds et al., 1996) provide point measurements over the years 1995–2016. The NOAA record is supplemented by archive tank measurements (in either stainless steel or treated aluminium tanks) at NWR spanning the years 1995–2022.

2.2 Sampling and analysis

2.2.1 AGAGE measurements

The majority of AGAGE DCE measurements were conducted using a Medusa preconcentration unit, coupled to gas chromatography and mass spectrometry (Medusa-GC/MS). The method is described in detail by Miller et al. (2008), Arnold et al. (2012), and Prinn et al. (2018) and only the most important aspects are summarized here. For some additional operational and analytical information see Appendix C.

With Medusa-GC/MS systems, one measurement is made every 60–65 min. Working standard measurements (std_sample) are either run after every air measurement (i.e. air_sample, std_sample, air_sample, std_sample) or after every two air measurements (i.e. air_sample, air_sample, std_sample, air_sample, air_sample, std_sample), with the latter approach used at JFJ, CMN, TOB, TAC, and in later years at CGO. For AGAGE in situ measurements, ambient air is sampled through inert, continuously flushed Synflex (Eaton) or stainless-steel inlet lines pumped from the top of an air sampling tower. From these continuous air streams, the air is sampled into the instruments using either a clean diaphragm or metal bellows pump. The sampling setups were found to not influence ambient levels of DCE.

With a Medusa-GC/MS, 2 L of air are sampled at a flow rate of 100 mL min^{-1} (i.e. total sampling time 20 min), dried using two Nafion membrane dryers (Perma Pure), and pre-concentrated and focused cryogenically with a two-trap system (Hayesep D adsorbent). For this, initially Polycold "Cryotiger"/PCC cryocoolers were used, which were eventually replaced by Stirling coolers (AMETEK, Inc./Sunpower Inc., CryoTel GT) at most sites, creating sample trapping temperatures of –165 °C or colder for both micro traps. More abundant bulk gases such as N_2, O_2, CO_2, and some noble gases, are largely removed from the sample via fractionated distillation steps (by controlled heating of each micro-trap) and purging with research grade helium. After pre-concentration, the analytes are cryo-focused and then transferred into a gas chromatograph (Agilent 6890, 7890). Chromatographic separation of DCE from other analytes is achieved with a CP-PoraBOND Q column (0.32 mm ID x 25 m, 5 µm film thickness; Agilent). The analytes are detected by electron ionization quadrupole mass spectrometry (EI)-qMS (Agilent 5975, 5977) in the selected ion monitoring (SIM) mode.

At CMN, the first years of the DCE record were measured using a simpler Adsorption Desorption System (ADS) (Maione et al., 2013), before the installation of a Medusa-GC/MS in December 2023. More details are described in Appendix C and Appendix D.

Helium (grade 5.0 or 6.0), which is further purified with a helium purifier (HP2, VICI), is generally used as the carrier gas. GCWerks (GCWerks, 2026) is used as instrument control and data processing software. Measured DCE mole fractions are reported as dry air mole fractions in ppt (parts per trillion, pmol mol^{-1}).

Laboratory air and "blank" samples are typically measured on a weekly basis. Laboratory air is monitored to identify cases where there is the potential for contamination of the ambient air samples. The blank measurements are performed by running a measurement cycle without trapping any sample air. In general, non-zero blanks can be indicative of contamination in the carrier gas, contamination or leakage within the instrument, or carry-over from the previous sample. For DCE we typically

observe non-zero blank values at all sites within the network except for CGO (this site only recorded a very small number of non-zero blanks over the entire timeseries). Carry-over has been identified as the principal cause of non-zero blanks for this species.

A correction was applied within the GCWerks software to account for non-zero blanks. This correction assumes that a constant blank mole fraction is added to all run types (e.g. blank, air, working standard). Typically, this is calculated as the mean mole fraction for the blank runs over each working standard lifetime (i.e. each physical working standard tank is associated with its own blank mole fraction). This correction performs well when the mole fraction of the ambient air is similar in magnitude to the mole fractions of the working standard and tertiary tank used to propagate the calibration scale to the site (see Sect. 2.3). For sites that experience very high pollution events, the assumption of a constant blank mole fraction breaks down. For example, the carry-over from a highly polluted air sample can significantly increase the peak area measured by the subsequent standard, such that the mole fraction calculated for the polluted air sample is underestimated. For this reason, data from the highly polluted AGAGE site at Gosan were excluded from this study, as the blank correction we applied could not account for carry-over in this case. The second most polluted site within the network for which DCE data exists was TAC. At this site the root-mean-squared error on the reported mole fractions due to carry-over was found to be 0.7 %. For 99 % of samples at this site, the impact of carry-over was found to be less than 2 %.

2.2.2 NOAA measurements

For NOAA's flask measurements, samples were collected approximately weekly during clean air conditions. Sample collection systems vary between sites, but the equipment used was found to not influence ambient air mole fractions of DCE during sampling. Intake heights vary from just a few meters above ground level (a.g.l.) at a high alpine tundra location (NWR), to 300 m a.g.l. (LEF). Most of the sampling inlets at the remote sites are between 10 and 20 m a.g.l. The intake lines are either continuously flushed Synflex (similar to the Medusa systems described above), 316 Stainless Steel, or polyvinylidene fluoride (PVDF; Kynar®) tubing that has been cleaned and baked in the laboratory prior to deployment to the field. These flushed intake lines are connected to a diaphragm pump (N86, KNF) with a 316 stainless-steel head and typically flow at 4–5 SLPM. The lines are flushed for 5–10 minutes (depending on measured flows at the site and inlet length) prior to connecting flasks to adequately flush out stagnant air before sampling is started. Paired 3 L internally electropolished stainless steel flasks are connected, and flushed for 12–20 minutes, again depending on the flow rate measured at the time of sampling (approximately 10 times the volume for two flasks combined). The flasks are flushed either in parallel, or in series (again site dependent) and subsequently pressurized to 3 bar absolute. The flasks are then shipped back to NOAA's Global Monitoring Laboratory in Boulder, Colorado, USA for analysis on the NOAA "M3" GC/MS (Agilent 6890 GC and Agilent 5973 MS) or, after November of 2023, the "M4" instrument (Agilent 8890 GC and 5977B MS).

For analysis, air from a flask is used to pre-flush the instrument inlet and approximately 200 mL (STP) of sample is directed onto a 10 cm length of a 0.53 mm ID uncoated fused silica tube maintained at reduced pressure and –165 °C. Prior to cryo-condensation of DCE and other trace analytes, the sample air is dried by passing it through a tube (~¼" SS by 10 cm long)

containing powdered magnesium perchlorate held in place with silanised glass wool. For the manually filled glass and stainless steel flasks, two injections are analysed from each flask, and the mean of four injections is reported for each sampling event. When flask pair differences are larger than 0.5 ppt or 10 % the results are discarded as being unreliable (less than 3 % of flask pairs). Only one injection is taken per flask from the automatically filled glass flasks, since a smaller amount of air is captured (0.7 L flasks are filled to 40 psia). Air analysis proceeds on a fused silica capillary column (0.25 mm ID x 60 m, with a 1 μm DB-5 film) that is cycled from –55 to 200 °C for each sample and by monitoring the ion at m/z = 62 ($C_2H_3Cl^+$). Peaks are integrated and peak area data are processed with custom software. Replicate injections from flasks are bracketed by analyses of working standards containing whole air, and instrument blanks (synthetic "zero" air) are analysed daily and have repeatedly shown no measurable levels of DCE. The median replicate injection precision (as 1 standard deviation of the two injections) in the ~10,000 flasks analysed over the measurement period has been 0.04 ppt (or 0.4 %); in 95 % of the analyses, it has been smaller than 0.16 ppt (2.3 %).

2.3 Calibration

2.3.1 AGAGE calibration approach

AGAGE's DCE measurements are linked to the recently established METAS-2021 primary calibration scale, which was produced based on permeation and dynamic dilution at the Swiss Federal Institute of Metrology (METAS). The measurement uncertainty on the SI-traceable mole fraction is 0.9 % (1-sigma confidence level, for cylinder MP21-001) (Bühlmann et al., in prep.; Guillevic et al., 2018). The integration of the METAS-2021 primary scale into the AGAGE R1 relative calibration scale (maintained by the Scripps Institution of Oceanography, SIO), allows full, network-wide intercalibration of DCE measurements. The primary scale is propagated to each AGAGE measurement site through a calibration scheme (Miller et al., 2008; Prinn et al., 2000, 2018) involving a set of three-level hierarchically linked standards. This calibration hierarchy comprises of: whole-air secondary standards, based at the SIO central calibration centre; whole-air tertiary standards, distributed to the sites by the calibration centre; and whole-air quaternary (working) standards, mostly collected by each group operating a measurement site. All whole-air standards are ambient moist air compressed into 34 L internally electro-polished stainless-steel tanks (Essex Industries, Inc.), using an oil-free diving air compressor (SA-6, RIX Industries), or collected cryogenically, during relatively clean air conditions. From the beginning of whole-air standard collection for the routine measurement of DCE in AGAGE (starting end of 2017), the ambient air at all sites contained DCE at mole fractions well above the limit of detections of onsite instrumentation. The accuracy associated with the propagation of the primary scale through the AGAGE calibration hierarchy is usually derived from propagating the measurement precisions.

The instrumental precisions for the in situ air measurements are derived from the standard deviations of continuously bracketing working standard measurements (see Sect. 2.2). During routine operation at each field site, working standard measurements bracket each or each pair of ambient air sample measurements to account for changes of the MS sensitivity. For Medusa-GC/MS instruments the average measurement precision for DCE was 0.5 % (taken as the mean of the average

precisions for each site). For the ADS instrument the respective average measurement precision was 1.6 %. Combining these on-site measurement precisions with uncertainties associated with the production and propagation of the calibration scale, including an estimate for the impact of carry-over of 0.7 % for each propagation step, we derive overall 1-sigma uncertainties of 2.4 % for the Medusa-GC/MS instruments; and 3.3 % for the CMN-ADS.

Weekly measurements of the working standard against the tertiary standard (typically 4 repeat sets of measurements) allow for tracking of potential drift of DCE in the standard cylinders. When a new tertiary standard arrives at a field site, it is compared to the old tertiary, and the old tertiary is remeasured at SIO, resulting in three sets of comparisons (OUT value at SIO, on-site value, IN value at SIO). Combined, these comparisons usually allow SIO to correct any drift in DCE (if it occurred). No drift has been observed in the secondary standards at SIO.

2.3.2 NOAA calibration approach

NOAA's DCE measurements are referenced to the NOAA-2003 absolute calibration scale, which consists of five different primary standards prepared using gravimetric techniques at mole fractions ranging from 13 to 30 ppt in Essex cannisters initially pressurized with humidified synthetic air to 900 psi. The response per mole of DCE injected for these standards in repeat analyses at different times has been within ± 5 % and has been consistent overall since they were initially prepared at different times between 2018 and 2022. Consistency in the measurement scale throughout the entire record is supported by repeat analyses of archived whole-air samples pressurized in Essex cryogenics 34 L cannisters. Repeat analyses for these archived samples has been within 5 % for the entire suite of samples, whose mole fractions range from 2 to 35 ppt. For more details on standard preparation in general at NOAA/GML, see Hall et al. (2007).

2.3.3 Network comparison

The measurements of both networks at five shared sites (CGO, SMO, RPB, THD, MHD) are regularly compared at the twice-yearly AGAGE meetings. For DCE, the average ratio between the NOAA (NOAA-2003 scale) and AGAGE (METAS-2021 scale) measurements is 1.0406 ± 0.0103 (NOAA/AGAGE) for the period 2017–2025.

2.4 Emissions modelling

2.4.1 Prior emissions

The global and regional emission estimates used a prior emissions map taken from Hossaini et al. (2024). In that study, several emissions maps were constructed by combining proprietary country-level data for DCE production with publicly available data for country-level imports and exports, then applying a range of different assumed production emission factors. Hossaini et al. (2024) established the scenario "sc05" map as their central case, as derived model results using sc05 were in overall better agreement with previous aircraft observations than for their other scenarios. Hence, in this study we use their scenario sc05 map, corresponding to emission factors from production of 0.5 % for developed countries and 1.5 % for developing

countries (as defined by Article 5 of the Montreal Protocol), with an emission factor of 0.1 % applied to imports (i.e. supply chain emissions) and consumption (assumed to be feedstock use). Emissions within each country were spatially distributed using an ethene proxy, taken from the "industrial combustion and processes" sector of the gridded (0.5°×0.5°) CMIP6 dataset (Feng et al., 2020). The Hossaini et al. (2024) emissions estimates only include years up to 2020, so for 2021–2023 we have used the 2020 emissions map.

2.4.2 Global modelling

Global emissions of DCE have been quantified using the approach described in detail in Western et al. (2025). In brief, an inverse method is used to derive emissions based on semi-hemispheric monthly averaged mole fractions and a 12-box model of the atmosphere (Cunnold et al., 1983; Rigby et al., 2014). The atmospheric lifetime of DCE is assumed to be controlled by reaction with the hydroxyl radical, with rate constants taken from Burkholder et al. (2020), and an ocean sink with a partial lifetime of 12.9 years (Yvon-Lewis and Butler, 2002). Given the errors likely introduced by using a coarse resolution atmospheric model for a short-lived substance, we assume a 1-sigma error of 50 % in the derived total effective lifetime, given the variability within each semi-hemisphere. The inverse method requires a-priori emissions, the "sc05" scenario from Hossaini et al. (2024) as described above, and we assume that the uncertainty in the year-to-year growth is 20 %. The measurement uncertainty is split into two components: a random 1-sigma uncertainty on the monthly mean mole fractions that combines uncertainties associated with propagating the scale from SIO to the AGAGE working standards (1.2 %) and the variability of the background measurements each month, and a systematic 1-sigma uncertainty associated with the calibration scale of 2.9 % (derived from the comparison between METAS-2021 and NOAA-2003 scales). In addition to providing posterior emissions estimates, posterior semi-hemispheric monthly mean mole fractions are also output by the model.

The global model results presented in the main text used only data collected as part of the core AGAGE and NOAA networks, with separate model runs performed using data from each network to independently derive emissions for the period 2017–2023. For this period the global emission growth rate is well constrained by the observational network. A separate model run was performed using the archived air measurements to derive emissions from 2002 onwards. Due to the sparsity of the air archive data, AGAGE and NOAA air archive measurements were both used simultaneously alongside core AGAGE measurements (after converting the NOAA data to the METAS-2021 scale using the average ratio of time-matched NOAA/AGAGE measurements at the co-located sites). Using these archive measurements allows for a comparison against the full emission timeseries presented by Hossaini et al. (2024), but the data sparsity leads to large uncertainty in the annual emission growth rate derived using the 12-box model. The results from these emissions estimates using the box model and air archive measurements are presented in Appendix E.

2.4.3 Regional modelling

DCE emissions in northwest (NW) Europe (Belgium, Germany, France, UK, Ireland, Luxembourg, and the Netherlands) and California were estimated using a regional modelling approach. For NW Europe, observations from the following sites were

used: CMN, JFJ, MHD, TAC, and TOB. The seven countries for which we report aggregate emissions were selected based on the country-level error reduction in the posterior relative to the prior. The California emission estimates used observations from the sites at SIO and THD. Four different inverse modelling systems were used for NW Europe: InTEM (Inverse Technique for Emission Modelling) (Arnold et al., 2018; Manning et al., 2021), RHIME (Regional Hierarchical Inverse Modelling Environment) (Ganesan et al., 2014), ELRIS (Empa Lagrangian Regional Inversion System) (Henne et al., 2016; Katharopoulos et al., 2023) and FLEXINVERT (Thompson and Stohl, 2014). Only InTEM and RHIME were used to estimate California emissions.

All four models employ Bayesian methods to infer emissions, subject to constraints provided by model and measurement uncertainties as well as uncertainties associated with a prior emissions map. The InTEM, RHIME, and ELRIS runs in this study all used the NAME (Numerical Atmospheric dispersion Modelling Environment) (Jones et al., 2007) dispersion model to represent the transport of emissions from their source to the measurement sites. FLEXINVERT used a different dispersion model: FLEXPART (FLEXible PARTicle dispersion model) (Bakels et al., 2024). All models used the Hossaini et al. (2024) prior map described above. Differences between the models are summarized in Appendix F (Table F1). In addition, a sensitivity test using a prior with uniform emissions over land was also performed for the NW Europe emission estimates, as described in Appendix F.

Details of the modelling approach used by InTEM, RHIME, and ELRIS are presented by Vollmer et al. (2026). Here we describe only the differences in model configuration for this specific study. In this case, the lifetime of DCE in the atmosphere is sufficiently long relative to the transport represented by the NAME model (up to 30 days backwards in time from each measurement point) that the species was considered inert within the model, in contrast to Vollmer et al. (2026), who applied a decay function to the model output to account for atmospheric degradation of the shorter-lived halogenated olefins in their study. The measurement uncertainties used by the models were taken to be the working standard precisions (as described in Sect. 2.3). Measurements were averaged into four-hour periods with the variability within each four-hour period used as a proxy for model representation uncertainty. The model and prior uncertainties used by each inversion system are described by Vollmer et al. (2026). In this study, RHIME used a scaling factor on the prior fluxes sampled from a lognormal distribution with a mean of 1 and a standard deviation of 8 (as opposed to a standard deviation of 4 used by Vollmer et al. (2026)), reflecting the higher uncertainty associated with the DCE prior flux map. Similarly, ELRIS used a spatial correlation length of 250 km for the prior emissions, as opposed to 500 km used by Vollmer et al. (2026), reflecting the expectation of more point-like sources and greater uncertainty on the prior spatial distribution for DCE.

In InTEM, boundary conditions were determined from the fraction of air entering from the 11 boundaries surrounding the computational domain (calculated by the NAME transport model) as detailed by Manning et al. (2021). Air entering from the southern boundaries is strongly influenced by the tropics and Southern Hemisphere, hence an average annual ratio of the background mole fraction between the northern tropics and the northern mid-latitudes was calculated from the observations at RPB, and the observations at MHD. The same estimated tropics ratio values were used for both the European and Californian domains. In RHIME and ELRIS, boundary conditions for the NW Europe estimates followed the same approach as Vollmer

et al. (2026). RHIME used prior boundary conditions for the California emission estimates taken from the results of the 12-box model (see Sect. 2.4.2).

In contrast to the other three models, FLEXINVERT employed the FLEXPART dispersion model with 10-day back-trajectory calculations (with DCE again assumed inert over this time frame). The measurements used in the inversion were averaged into three-hour periods (different from the four-hour averaging of the other models). The FLEXINVERT inversion framework used is detailed by Annadate et al. (2025); here, we focus only on the details specific to this study. For the estimation of background mole fractions, we applied the Robust Extraction of Baseline Signal (REBS) (Ruckstuhl et al., 2012) method. Within the FLEXINVERT+ framework, we utilised a log-normal prior emission distribution and the M1QN3 solver to iteratively minimize the cost function. To estimate posterior uncertainties, we ran a 20-member Monte Carlo ensemble of inversions.

3 Results and discussion

3.1 Atmospheric mole fractions

Fully calibrated measurements started for most NOAA sites at the beginning of 2017 and for most AGAGE sites towards the end of 2017. A list of measurement sites is given in Appendix B, and the observations up to the end of 2023 are shown in Fig. 2 and Fig. 3. Since the start of the ongoing measurement record, DCE was detectable in the atmosphere at all sites. The 12-box model posterior global mean mole fractions are 6.58 ± 0.27 ppt for AGAGE, and 7.50 ± 0.28 ppt for NOAA over the 7-year reporting period (plot shown in Appendix E). There is not a monotonic trend in the annual average global atmospheric abundance over this period. We observe growth between 2017 and 2018/2019, followed by a decline until 2022, returning to growth from 2022 to 2023. This may reflect changes in emissions (see Sect. 3.2), although any changes in the DCE sink over this time period could also contribute.

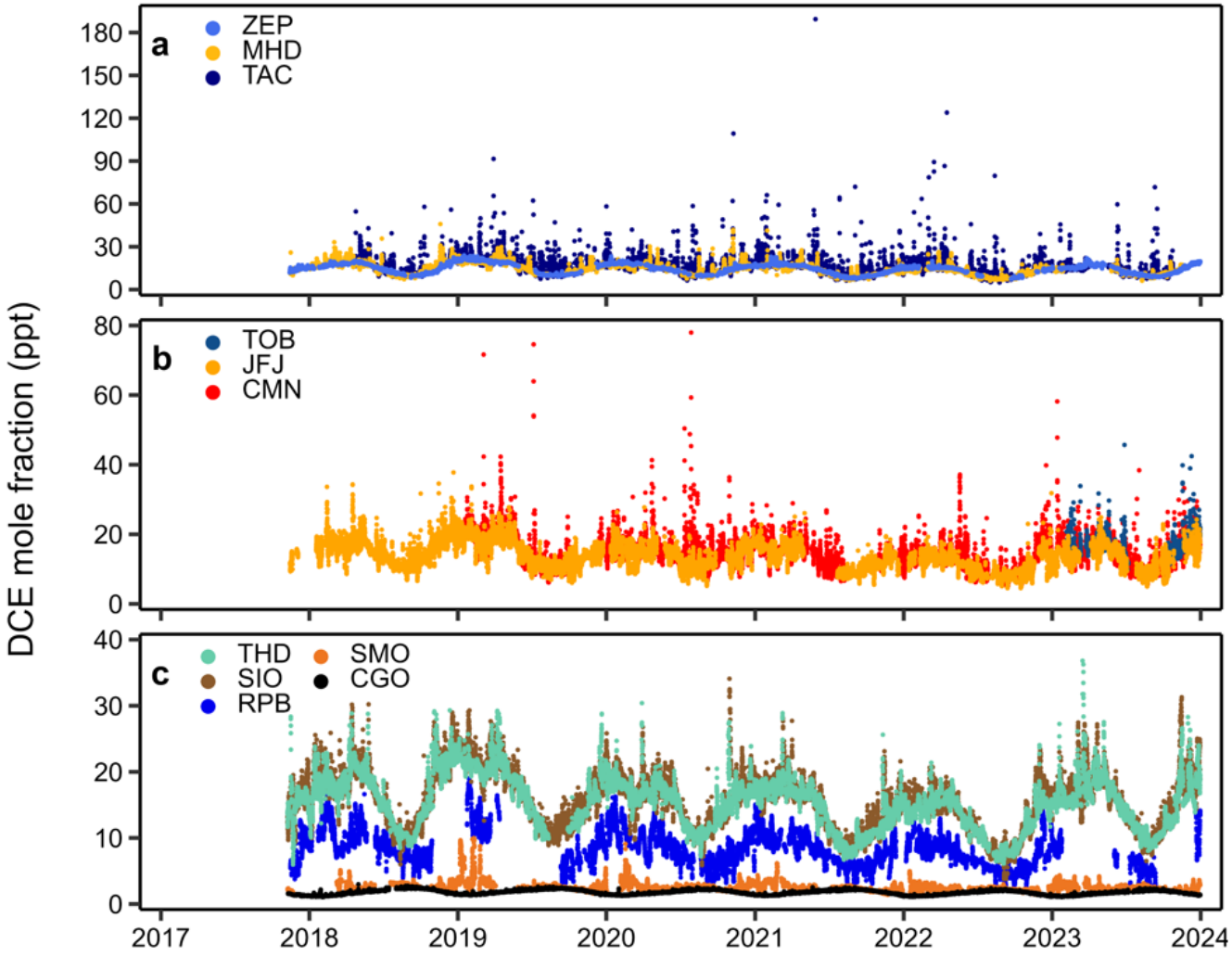

345 **Figure 2. In situ observations of 1,2-dichloroethane (DCE) at AGAGE stations. For better visualisation, the records are shown on different panels, in the order of the site latitudes. a) Zeppelin, Svalbard, Norway (ZEP); Mace Head, Ireland (MHD); Tacolneston, UK (TAC). b) Taunus, Germany (TOB); Jungfraujoch, Switzerland (JFJ); Monte Cimone, Italy (CMN). c) Trinidad Head, California, USA (THD); Scripps Institution of Oceanography, California, USA (SIO); Ragged Point, Barbados (RPB); Cape Matatula, American Samoa (SMO); Kennaook/Cape Grim, Tasmania, Australia (CGO).**

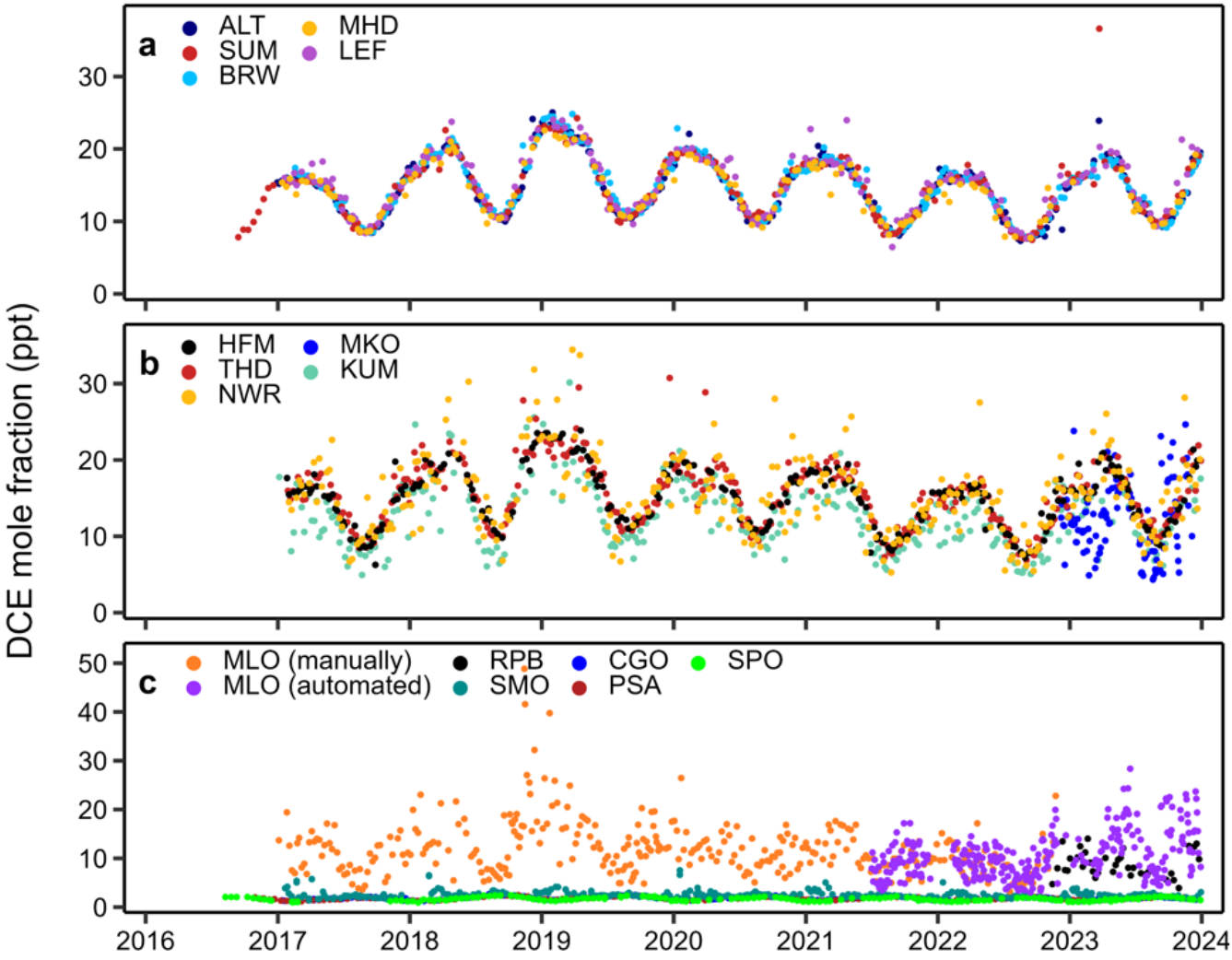

Figure 3. Flask measurements of 1,2-dichloroethane (DCE) from NOAA stations visualised as flask pair means. For better visualisation, the records are shown on different panels, in the order of the site latitudes. a) Alert, Canada (ALT); Summit, Greenland (SUM); Barrow, Alaska, USA (BRW); Mace Head, Ireland (MHD); Park Falls, Wisconsin, USA (LEF). b) Harvard Forest, Massachusetts, USA (HFM); Trinidad Head, California, USA (THD); Niwot Ridge, Colorado, USA (NWR); Mauna Kea, Hawaii, USA (MKO); Cape Kumukahi, Hawaii, USA (KUM). c) Mauna Loa, Hawaii, USA (MLO); Ragged Point, Barbados (RPB); Cape Matatula, American Samoa (SMO); Kennaook/Cape Grim, Tasmania, Australia (CGO); Palmer Station, Antarctica (PSA); South Pole, Antarctica (SPO).

The observations show large spatial and temporal variations. As for most other synthetic halogenated gases, there is a clear hemispheric difference in the atmospheric abundance. This is especially pronounced for short-lived gases such as DCE, for which the Northern Hemisphere mean mole fractions are approximately 5 times higher than those in the Southern Hemisphere. While observed mole fractions at CGO and at the two Antarctic sites (PSA and SPO) are in the range 1–3 ppt, and little

deviation from the seasonally-varying baseline is observed, the further north the sites in the tropical zone are located, the higher the baseline level of the observations. In the northern hemisphere, observed baseline monthly-mean mole fractions range between a minimum of 4 ppt and a maximum of 27 ppt (with a standard deviation of 4 ppt across both the AGAGE network and NOAA network), which is consistent with boundary layer mole fractions previously reported from aircraft campaigns (Engel and Rigby et al., 2018; Roozitalab et al., 2024).

NOAA flask samples are typically collected under background conditions, although several samples at MLO were found to be elevated above baseline due to the influence of East Asian outflow. In contrast the in situ AGAGE data show pronounced pollution events (deviations from the baseline level) at several northern hemispheric sites. In particular, mole fractions more than twice the baseline value were frequently observed at TAC, with extreme events exceeding 100 ppt. These events reflect the proximity of this site to known producers and users of DCE (see Sect. 3.3). CMN is the next most polluted site, followed by MHD and TOB. No other AGAGE site observed mole fractions exceeding 40 ppt.

Although the global production volume of DCE is by far the largest among the Cl-VSLS regularly measured and publicly reported by the two networks, the global mean mole fractions (estimated directly from the measurements or from the model posterior) of DCE are third highest. The 12-box model global average mole fractions for DCE in 2020 (6.7 ppt (AGAGE) and 7.7 ppt (NOAA)) sit between those of DCM (38.3 ppt (AGAGE) and 45.5 ppt (NOAA)) (Laube and Tegtmeier et al., 2022) and PCE (1.01 ppt (AGAGE) and 1.12 ppt (NOAA)) (Laube and Tegtmeier et al., 2022), and are approximately of the same magnitude as CFM (8.7 ppt (AGAGE)) (Laube and Tegtmeier et al., 2022).

Measurements of DCE in archive tanks filled at THD, CGO, and NWR, as well as flask samples from the KSG Station, are shown in Fig. 4. Samples were measured at either Empa or NOAA (see Fig. 4 legend). The mole fractions have been corrected to represent annual average values. For the NOAA samples at NWR, this correction was performed using the average ratio of monthly means to running annual means derived from the ongoing measurements at NWR during 2017–2023. For THD and CGO, a Savitzky–Golay filter (Savitzky and Golay, 1964) (window length = 60 days, polynomial order = 2) was applied to the in situ mole fractions to generate a smoothed seasonal cycle for each site as a function of day-of-year. The normalised seasonal cycle for each site was used to correct the archive data, and the KSG flasks were corrected using the normalised CGO seasonal cycle. To enable direct comparison of all measurements, NOAA measurements have been converted to the METAS-2021 scale by dividing all mole fractions by 1.0406 (the average ratio of time-matched NOAA/AGAGE measurements at the co-located sites: CGO, SMO, RPB, THD, MHD). Annual average in situ data are also shown for THD and CGO.

The northern hemisphere sites (THD and NWR) show increasing mole fractions for about a decade starting in 2002. Before and after that period the trend is less clear. Global emissions estimates for 2002 onwards based on these archive measurements are presented and discussed in Appendix E.

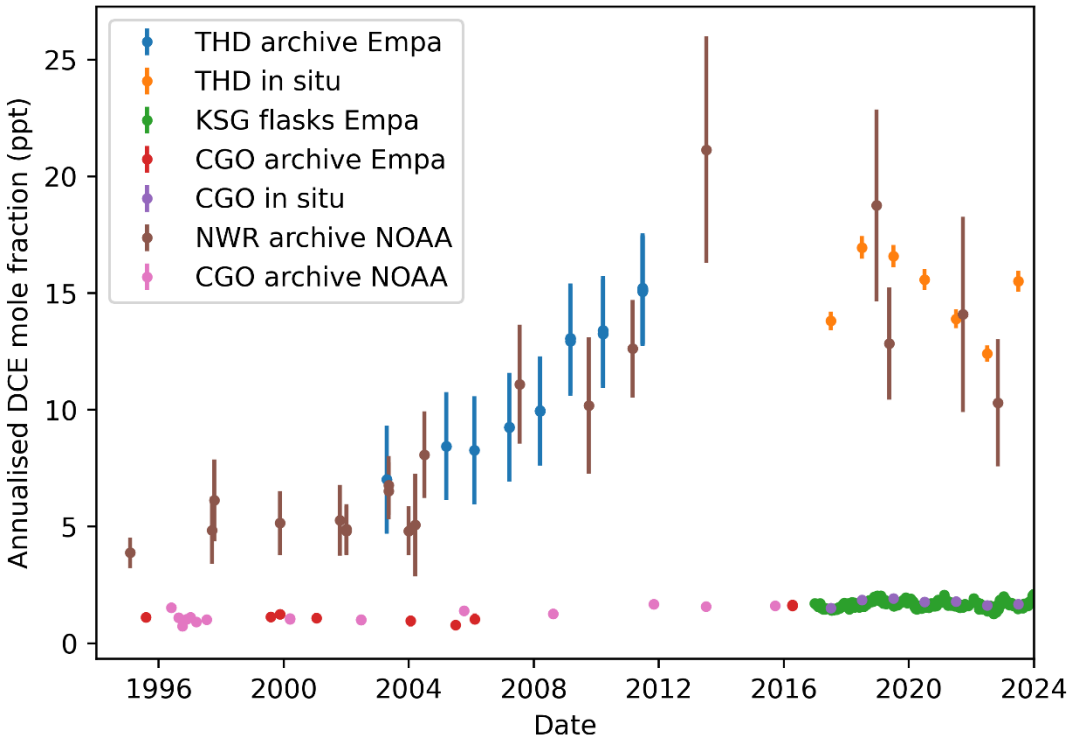

Figure 4. Annualised 1,2-dichloroethane (DCE) mole fractions measured in archive tanks filled at Trinidad Head, California, USA (THD); Kennaook/Cape Grim, Tasmania, Australia (CGO); and Niwot Ridge, Colorado, USA (NWR); and flask samples from the King Sejong Station, Antarctica (KSG). Annual mean in situ mole fractions from THD and CGO are also shown. Archive and flask samples were analysed at either Empa or NOAA as indicated in the legend. Error bars represent uncertainties due to measurement precision, seasonality correction and calibration scale. For KSG and CGO these uncertainties are too small to be visible on this scale. Measurements at NOAA have been converted to the METAS-2021 scale using the average ratio of NOAA versus AGAGE measurements at co-located sites (i.e. they were divided by 1.0406).

3.2 Global emissions

Estimated global annual emissions are shown in Fig. 5. Over all years covered by this study (2017–2023) mean emissions are 453 ± 185 Gg yr^{-1} (AGAGE) and 525 ± 209 Gg yr^{-1} (NOAA), with a decreasing trend observed between 2018 and 2022. The large uncertainties on these results stem from the assumption of a 50 % uncertainty in the derived total effective lifetime of DCE. This represents a systematic uncertainty, which impacts the absolute emission magnitude and not the emission growth rate, as discussed further in Appendix E.

While the global emission estimates from NOAA and AGAGE are not significantly different, we expect some small differences based on two main factors. The first is the difference in calibration scale between the two networks (see Sect. 2.3), which

would systematically scale the emissions approximately proportionately to the ratio between the calibration scales (estimated to be 1.0406 based on the ratio of co-located NOAA/AGAGE measurements). Eliminating this calibration scale difference would bring results from the two networks into closer agreement, however the mean ratio of posterior emissions is 1.16 (NOAA/AGAGE), implying that there are other contributing factors. A second factor known to influence the 12-box model results is the difference in the spatial distribution of sampling between the two networks, as has been discussed previously for other Cl-VSLS (e.g., Carpenter and Reimann et al., 2014). The relative short lifetime of DCE can mean that backgrounds are not zonally homogeneous, and not approximately homogenous within a meridional semi-hemisphere. This challenges the assumptions made when using a simplistic 12-box model; however, the agreement between emissions derived using the AGAGE and NOAA networks, which have different sampling locations, suggest that the estimates are robust, considering the prescribed uncertainties. Efforts have been made to eliminate measurements in obviously polluted air masses from the global emission estimate. For example, there are times when measurements made at MLO and KUM are elevated above typical background levels (see Fig. 3), likely due to outflow from East Asia, as has been observed for other compounds (e.g., Montzka et al., 2018).

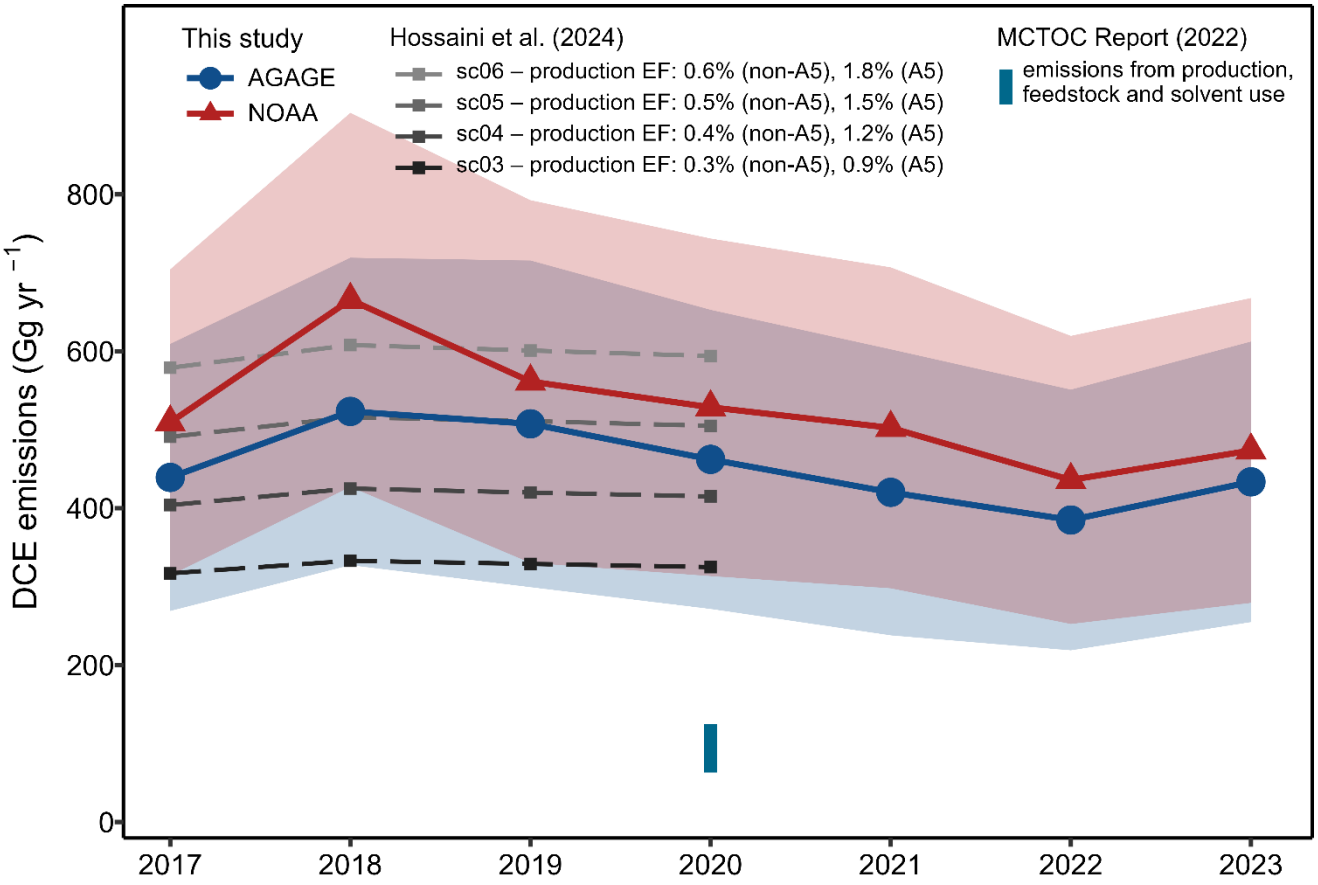

Figure 5. Global emissions of DCE derived from measurements from the AGAGE (blue line and points) and NOAA (red line and triangles) networks, using a 12-box model. Uncertainties of the global emissions (blue and red shaded bands) are given at 1-sigma confidence level. The derived emissions are compared to the emissions derived by Hossaini et al. (2024) for their different emission factor scenarios (sc; dashed lines in different grey shades). In that study, sc03 uses an emission factor from production of 0.3 % (non-Article 5 countries) and 0.9 % (Article 5 countries), sc04 uses corresponding factors of 0.4 % and 1.2 %, and so on. The derived emissions are also compared to an emissions estimate reported by the Medical and Technical Options Committee (MCTOC; UNEP, 2022).

The years 2017–2020 covered by our study overlap with the investigation period of Hossaini et al. (2024). Our derived global emissions from both networks fit well to the emissions magnitudes of scenarios 4 (sc04) to 6 (sc06) described in their study. Scenario 4 assumes emission factors during production of 0.4 % (developed/non-Article 5 countries) and 1.2 % (developing/Article 5 countries), while sc05 uses factors of 0.5 % and 1.5 %, and sc06 uses factors of 0.6 % and 1.8 %, respectively. For fugitive emissions from the supply chain (imports) and feedstock uses, a fixed emission factor of 0.1 % was assumed. This resulted in mean 2017–2020 global emissions of 416 Gg yr^{-1} (sc04), 506 Gg yr^{-1} (sc05), and 596 Gg yr^{-1} (sc06). In line with the findings of Hossaini et al. (2024), our results suggest a potential stabilisation (or even a slight decrease) in emissions in recent years, following two decades of steady growth implied from their analysis of production statistics and trade data (and broadly consistent with our archive measurements). The decrease in emissions between 2018 and 2020 observed in our results is larger than the corresponding decrease in the Hossaini et al. (2024) scenarios. Improved abatement measures could play a role in this discrepancy, as they would reduce the average global emission factors from DCE production over time. Similarly, a reduction in emissions during feedstock use or transport of DCE could contribute (especially if these sources constitute a larger share of global emissions than assumed by Hossaini et al. (2024)), as could a reduction in solvent use of DCE (a source that is not included in the Hossaini et al. (2024) scenarios). Extending both the bottom-up inventory estimates and the top-down 12-box model estimates to future years would enable a better assessment of whether systematic changes in these DCE emission sources are indeed occurring.

Compared to our results and the previous observationally-constrained study (Hossaini et al., 2024), the Medical and Technical Options Committee (MCTOC) Assessment Report (2022) (UNEP, 2022) estimated notably lower global DCE emissions for 2020 of 60–105 Gg yr^{-1}, assuming low emission factors for production, transport, and storage, plus an additional 3–20 Gg yr^{-1} from solvent use (UNEP, 2022).

Of all reported VSLS emissions for 2020, calculated using the global 12-box model, our derived global DCE emissions are second highest. For 2020, they compare to global emissions of DCM of 1130 ± 211 Gg yr^{-1} (AGAGE) or 1328 ± 242 Gg yr^{-1} (NOAA); of CFM of 339 ± 70 Gg yr^{-1} (AGAGE); and of PCE of 80 ± 39 Gg yr^{-1} (AGAGE) or 91 ± 47 Gg yr^{-1} (NOAA) (Laube and Tegtmeier et al., 2022). Despite being produced in higher amounts than DCM, DCE is less dominantly used in directly emissive applications (UNEP, 2022).

3.3 Regional emissions

Emission estimates for NW Europe and California are shown in Fig. 6. The mean posterior emission estimates (over all models and years) are 2.06 [1.31, 2.65] Gg yr^{-1} for NW Europe and 0.23 [0, 0.37] Gg yr^{-1} for California (where the uncertainty bounds

represent the range between the lowest 15.9 percentile and the highest 84.1 percentile for any of the individual models). In both cases these emission estimates represent less than 0.5 % of the global total emissions. There is no significant overall temporal trend in either region. In both cases the posterior estimates are much lower than the prior emissions of 47.9 Gg yr^{-1} (NW Europe) and 15.4 Gg yr^{-1} (California) taken from Hossaini et al. (2024), and in California they are statistically indistinguishable from zero. This implies some combination of two factors:

1. The country-level totals from Hossaini et al. (2024) sc05 are too high for these regions.
2. The distribution of DCE emissions within individual countries is not well approximated by the ethene emissions map (Feng et al., 2020) used as a proxy in deriving their gridded emissions.

Factor 2) is likely to be particularly consequential for California, as the USA Environmental Protection Agency (EPA) Chemical Data Reporting (CDR) (EPA, 2025b) does not list any facilities within the state either producing or using DCE, whereas the gridded ethene emissions on which our prior is based do contain significant Californian emissions. Due to the limited spatial sensitivity of our measurement sites, particularly in regions where substantial industrial production of chlorinated chemicals is known to occur, we are unable to estimate country-level emissions for the whole USA.

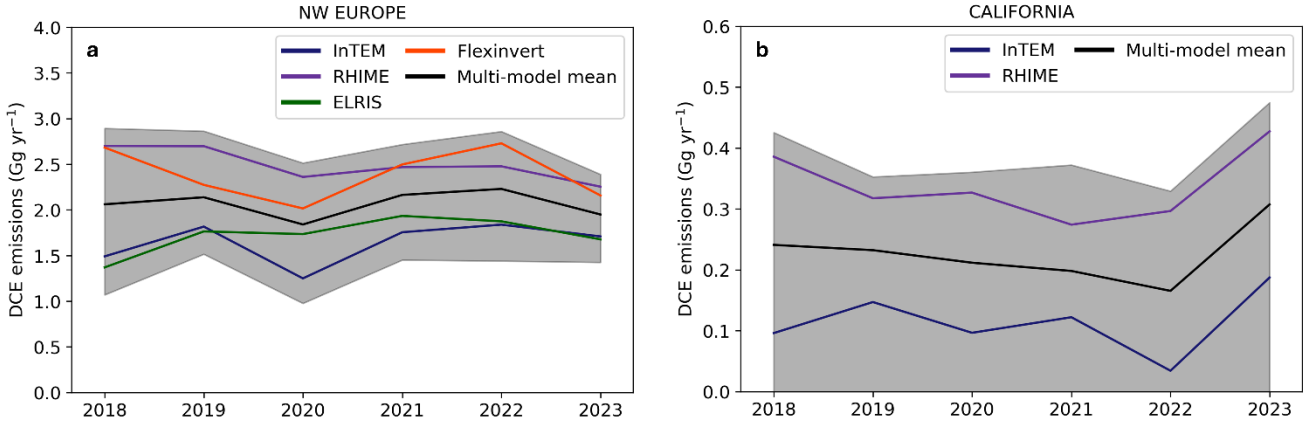

Figure 6. Regional inverse modelling results of 1,2-dichloroethane (DCE) emissions for NW Europe (a) and California (b). The coloured lines represent individual model results, and the black line represents the multi-model mean. The grey shading represents the range between the lowest 15.9 percentile and the highest 84.1 percentile for any of the individual models.

Our gridded emission maps (Fig. 7) show that NW Europe also has a different spatial distribution in the posterior compared to the prior. However, because our NW Europe region consists of seven countries, our posterior estimates also reflect lower country-level totals than the prior. This in turn implies that either the activity data (i.e. production and import/export data) and/or the emission factors (production = 0.5 %, feedstock use = 0.1 %, supply chain leakage = 0.1 %) used by Hossaini et al. (2024) sc05 are overestimates for the countries in this region. When interpreting this discrepancy, it is worth considering the spatial sensitivity of the observations used by Hossaini et al. (2024) to select the sc05 production emission factors as their central case. These data are from aircraft campaigns designed to make representative measurements of background air over

the Pacific and Atlantic Oceans, covering a wide range of latitudes, thus making them well suited to evaluating global models. The sensitivity of this dataset to emissions from NW Europe is limited, so while sc05 may be globally optimal, regional variability in these emission factors can be expected due to differences in technology and regulatory regimes.

The posterior emission maps in NW Europe show emissions concentrated around facilities known to be large producers and/or users of DCE. While it is not possible to estimate emissions at the facility level using this regional modelling approach, the fact that the posterior maps locate the emissions at these likely sources (without being passed information regarding their locations in the prior) is noteworthy. Operators of industrial facilities undertaking certain activities within the European Union must report their atmospheric emissions of DCE to the European Pollutant Release and Transfer Register (E-PRTR; EEA, 2026) when they exceed 1000 kg yr^{-1}. Since the UK left the European Union, UK facilities have reported instead to the UK Pollutant Release and Transfer Register (UK-PRTR; DEFRA, 2012). Combining the two datasets, we obtain total reported emissions for NW Europe of 0.78 Gg yr^{-1} when averaged over the years 2018–2023, with a minimum annual value of 0.62 Gg in 2023 and a maximum of 0.98 Gg in 2020 (see Appendix G for all annual values). These totals are lower than our top-down estimates, which is expected because these inventories do not include emissions from storage or transport, or from DCE producers/users whose emissions are below the reporting threshold.

Total emissions from the two regions modelled in this study are orders of magnitude lower than our global emission estimates, reflecting the fact that these regions are not significant emitters in the global context.

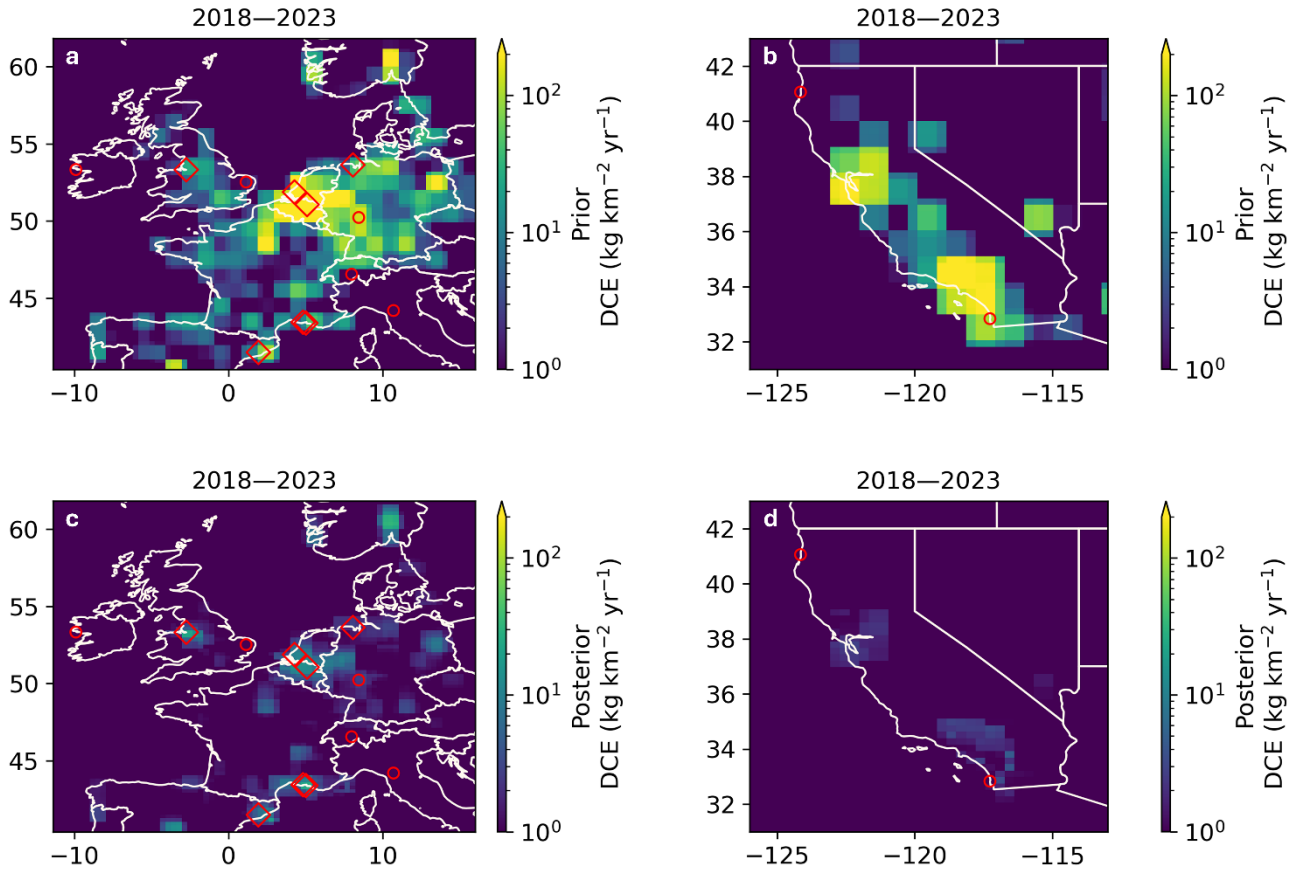

Figure 7. Prior (a, b) and mean posterior (c, d) maps of 1,2-dichloroethane (DCE) emissions for NW Europe (a, c) and California (b, d). The red circles denote the measurement sites, and the red diamonds show the locations of facilities known to be large producers and/or users of DCE. Note that a logarithmic colour scale is used in order to show features in both the prior and posterior maps on the same scale. .

4 Conclusions

We have presented ongoing surface-based observations of DCE from the AGAGE and NOAA global measurement networks, covering the years 2017–2023. Of the Cl-VSLS currently reported by those networks, the global production volume of DCE is the highest, with a primary use as a feedstock in PVC manufacture. The global mean atmospheric abundance was relatively constant over the study period. The observed baseline mole fractions were on the order of 1–3 ppt in the southern hemisphere, and on the order of 5–25 ppt in the northern hemisphere. Using AGAGE and NOAA archive measurements (sampled at three sites) we have extended the observation record back in time to the 1990s. These sporadic samples reveal a substantial increase in global DCE abundance since this time.

Based on the AGAGE and NOAA observations, we estimated global emissions for 2017–2023 of 453 ± 185 Gg yr^{-1} and 525 ± 209 Gg yr^{-1}, respectively, and there is no monotonic trend over these years (although emissions decreased between 2018 and 2022). These global DCE emissions are the second highest of the Cl-VSLS emissions inferred using the global 12-box model and reported by the two monitoring networks for 2020. Our calculated global DCE emissions are in good agreement (within uncertainties) with the recently published results of Hossaini et al. (2024), who used an observation-informed bottom-up approach.

Using AGAGE measurements, we also estimated regional emissions for NW Europe of 2.06 [1.31, 2.65] Gg yr^{-1} and for California of 0.23 [0, 0.37] Gg yr^{-1}, making these two regions small contributors to the total global emissions. These estimated regional emissions are at least an order of magnitude smaller than those in Hossaini et al. (2024). Hossaini et al. (2024) estimated that ~48 % of global emissions came from Asia in 2020. In addition to the production, supply chain and feedstock use emissions considered in their study, Hossaini et al. (2024) also hypothesise the presence of additional direct emissions due to solvent use, predominantly in regions where it is a lower-cost option and not restricted, such as in developing countries. Improving measurement coverage in Southeast Asia would help constrain emissions from this important region, particularly since ODPs for Southeast Asian DCE emissions have been estimated to be twice the global average due to the influence of deep convection associated with the monsoon (Adcock et al., 2020). Additional observations there and in other key source regions that currently have poor measurement coverage could be used in conjunction with a regional modelling approachto provide spatially resolved emission estimates. Such regional estimates are particularly important for DCE and other Cl-VSLS (relative to longer-lived species) because of their regionally varying ODPs.

Inventory accounting of DCE sources suggests that the future production, use, and emissions of DCE depend primarily on the anticipated growth in PVC demand in combination with employed manufacturing technologies, and on regulatory controls implemented in response to the toxicity of DCE (ECHA, 2022; EPA, 2020b, 2024, 2026; Sherwood, 2018; UNEP, 2022). The possibility of increasing future emissions of DCE – as inventory accounting and our archive measurements suggest happened in the past (Hossaini et al., 2024) – could result in an increased contribution to stratospheric chlorine and, hence, ozone depletion. In addition, despite the low direct ODP of DCE, its indirect ODP may be higher, as gases such as carbon tetrachloride (CCl_4) could be released during DCE manufacture (Hossaini et al., 2015; Reimann et al., 2026). Therefore, although the current impact of DCE and other anthropogenically emitted Cl-VSLS on ozone depletion is considered small, it could become relatively more important in the future (Chipperfield et al., 2020; Dubé et al., 2025) assuming that emissions of Montreal Protocol controlled ODSs keep declining. Continued atmospheric monitoring of DCE would allow a basis for continued assessment of emerging environmental and health impacts.

Code and data availability

Comment to the editor and the reviewers: The observations and full model output (which contains the observations) will not be made publicly available until acceptance for publication of the manuscript. However, all data will be made available to the

editor and the reviewers during the review process. Observations made by the AGAGE network are available from https://www-air.larc.nasa.gov/missions/agage/. Observations made by the NOAA network are available from https://www.gml.noaa.gov/data/. Additional flask and air archive data will be uploaded as a supplement (in the final submission). The code for RHIME is available at https://github.com/openghg/openghg_inversions. FLEXINVERT code can be downloaded from https://flexinvert.nilu.no. The code for InTEM and ELRIS are available on request. Code for the 12-box model and its inverse method are available at https://doi.org/10.5281/zenodo.6857446 (Rigby and Western, 2022b) and https://doi.org/10.5281/zenodo.6857794 (Rigby and Western, 2022a). Model data post-processing and plotting utilized the python package FLUXIE (Flux Intercomparison Environment) (Ramsden et al., 2025). All model output from this paper is available from xxxx (we will insert zenodo link here).

Author contributions

Measurements were made by MKV, JM, TB, CMH, SAM, BDH, IJV, DY, SOD, AW, CRL, OH, TW, AE, JA, MM, BM, BPK, PJF, JK, TSR, TGS, RFW and KMS. Data processing and quality assurance was conducted by JRP, DR, MKV, JM, TB, CMH, SAM, BDH, IJV, DY, SOD, AW, CRL, OH, TW, AE, JA, MM, JY, BM, PBK, PJF, JK, RHJW, TGS, RFW and KMS. The data acquisition and instrument control software was developed by PKS. Model development was done by JRP, AG, LMW, AJM, ALR, SH, DBM, SA, LC, BMM, MR, RGP. The model runs for this study were conducted by JRP, LMW, ALR, DBM, SA. Manuscript writing was led by DR and JRP, with contributions from most co-authors.

Competing interests

The authors declare that they have no competing interests.

Acknowledgements

We acknowledge all personnel of the measurement stations and in the laboratories for supporting the measurements made by AGAGE and NOAA. Financial support was provided as follows: for AGAGE principally by the National Aeronautics and Space Administration (NASA) Upper Atmosphere Research Program (grants 80NSSC21K1369 to MIT, grants 80NSSC21K1210 and 80NSSC21K1201 to SIO, several preceding grants for the lab operations at SIO and the support of Trinidad Head and Cape Matatula, and partial support of Ragged Point, Mace Head, and Kennaook/Cape Grim); for Cape Matatula by NOAA; for Mace Head and Tacolneston, as part of the UK DECC Network, by the UK Government's Department for Energy Security and Net Zero (DESNZ; contract nos. TRN1028/06/2015, TRN1537/06/2018, TRN5488/11/2021 and prj_1604 to the University of Bristol); for Ragged Point by NOAA (contracts RA-133-R15-CN-0008, 1305M319CNRMJ0028 and 1305M324P0411 to the University of Bristol); for Kennaook/Cape Grim by the Commonwealth Scientific and Industrial

Research Organization (CSIRO Australia), the Bureau of Meteorology (Australia), the Department of Climate Change, Energy, the Environment and Water (Australia), Refrigerant Reclaim Australia, the Australian Refrigeration Council, and through the NASA award to MIT with subaward to CSIRO for Cape Grim (80NSSC21K1369); for Jungfraujoch by the Swiss National Programs HALCLIM and CLIMGAS-CH (Swiss Federal Office for the Environment, FOEN) and by the International Foundation High Altitude Research Stations Jungfraujoch and Gornergrat (HFSJG); for Zeppelin by the Norwegian Environment Agency; for Monte Cimone by the Italian component of ACTRIS (Aerosol, Clouds and Trace Gases Research Infrastructure), under the Programma Operativo Nazionale Ricerca e Innovazione 2014–2020 PIR01 00015 "PER-ACTRIS-IT"; for Taunus by the German ACTRIS programme and by the PARIS (Process Attribution of Regional Emissions) EU Project (Grant Agreement 10108430); for Gosan by the National Research Foundation of Korea (NRF) grant funded by the Ministry of Science and ICT (No. RS-2023-00229318); for the King Sejong flask sample programme partially by the Korea Polar Research Institute's Antarctic Monitoring Program (PE26170), several preceding grants (PE13410 and PE20150) and earlier also by the Swiss State Secretariat for Education and Research and Innovation (SERI).

NOAA authors SAM, BDH, and IJV acknowledge the technical support of S. Clingan, M. Crotwell, G. Dutton, and K. Petersen for analysing flasks and for their handling of logistics associated with the sampling and analysis of flasks.

We acknowledge the support of TB's work within the project 19ENV06 MetClimVOC, which has received funding from the EMPIR programme, and within the project AtmoChemECV2 funded by METAS. We acknowledge the support of DR's work by the Greenhouse Gas Emissions Measurement and Modelling Advancement (GEMMA) Programme, funded by the UK Natural Environment Research Council (NERC). The regional inverse modelling was supported by a model development programme organized through PARIS, GEMMA and the Natural Environment Research Council (NERC) InHALE project (NE/X00452X/1). The RHIME model runs were carried out using the computational facilities of the Advanced Computing Research Centre, University of Bristol (http://www.bristol.ac.uk/acrc/). FLEXPART simulations were carried out at the Swiss National Supercomputing Centre (CSCS) under institutional contract ID em05. We thank Ryan Hossaini for helpful discussions about the approach taken to derive the DCE emission map we use as our prior, and its associated uncertainties.

References

Adcock, K. E., Fraser, P. J., Hall, B. D., and Langenfelds, R. L.: Aircraft-Based Observations of Ozone-Depleting Substances in the Upper Troposphere and Lower Stratosphere in and Above the Asian Summer Monsoon Journal of, Geophys. Res. Atmos., 126, 1–18, https://doi.org/10.1029/2020JD033137, 2020.

AGAGE: AGAGE: https://www-air.larc.nasa.gov/missions/agage/, last access 20 March 2026, 2025.

Annadate, S., Mancinelli, E., Gonella, B., Moricci, F., O'Doherty, S., Stanley, K., Young, D., Vollmer, M. K., Cesari, R., Falasca, S., Giostra, U., Maione, M., Arduini, J., and Giostra, U.: Monitoring the impact of EU F-gas regulation on HFC-134a emissions through a comparison of top-down and bottom-up estimates, Environ. Sci. Eur., 37, 1–12,

https://doi.org/10.1186/s12302-025-01081-1, 2025.

Arcoya, A., Cortés, A., and Seoane, X. L.: Tri- and Perchloroethylene. 1. Fluid Catalytic Oxyhydrochlorination of Ethylene, Ind. Eng. Chem. Prod. Res. Dev., 19, 77–82, 1980a.

Arcoya, A., Cortés, A., and Seoane, X. L.: Tri- and Perchloroethylene. 2. Fluid Catalytic Oxyhydrochlorination of Dichloroethane, Ind. Eng. Chem. Prod. Res. Dev., 19, 82–86, 1980b.

Arnold, T., Mühle, J., Salameh, P. K., Harth, C. M., Ivy, D. J., and Weiss, R. F.: Automated Measurement of Nitrogen Trifluoride in Ambient Air, Anal. Chem., 84, 4798–4804, https://doi.org/10.1021/ac300373e, 2012.

Arnold, T., Manning, A. J., Kim, J., Li, S., Webster, H., Thomson, D., Mühle, J., Weiss, R. F., Park, S., and O'Doherty, S.: Inverse modelling of CF_4 and NF_3 emissions in East Asia, Atmos. Chem. Phys., 18, 13305–13320, https://doi.org/10.5194/acp-18-13305-2018, 2018.

Ayres, R. U. and Ayres, L. W.: The Life Cycle of Chlorine, Part II: Conversion Processes and Use in the European Chemical Industry, J. Ind. Ecol., 1, 65–89, 1997.

Bakels, L., Tatsii, D., Tipka, A., Thompson, R., Dütsch, M., Blaschek, M., Seibert, P., Baier, K., Bucci, S., Cassiani, M., Eckhardt, S., Zwaaftink, C. G., Henne, S., Kaufmann, P., Lechner, V., Maurer, C., Mulder, M. D., Pisso, I., Plach, A., Subramanian, R., Vojta, M., and Stohl, A.: FLEXPART version 11: improved accuracy, efficiency, and flexibility, Geophys. Res. Lett., 17, 7595–7627, 2024.

Barletta, B., Meinardi, S., Simpson, I. J., Atlas, E. L., Beyersdorf, A. J., Baker, A. K., Blake, N. J., and Yang, M.: Characterization of volatile organic compounds (VOCs) in Asian and north American pollution plumes during INTEX-B: identification of specific Chinese air mass tracers, Atmos. Chem. Phys., 9, 5371–5388, 2009.

Bednarz, E. M., Hossaini, R., Chipperfield, M. P., Abraham, N. L., and Braesicke, P.: Atmospheric impacts of chlorinated very short-lived substances over the recent past – Part 1: Stratospheric chlorine budget and the role of transport, Atmos. Chem. Phys., 22, 10657–10676, https://doi.org/10.5194/acp-22-10657-2022, 2022.

Bednarz, E. M., Hossaini, R., and Chipperfield, M. P.: Atmospheric impacts of chlorinated very short-lived substances over the recent past – Part 2: Impacts on ozone, Atmos. Chem. Phys., 23, 13701–13711, https://doi.org/10.5194/acp-22-10657-2022, 2023.

Braesicke, P., Neu, J., Fioletov, V., Godin-Beekmann, S., Hubert, D., Petropavlovskikh, I., Shiotani, M., Sinnhuber, B.-M., Ball, W., Chang, K.-L., Damadeo, R., Dhomse, S., Frith, S., Gaudel, A., Hassler, B., Hossaini, R., Kremser, S., Misios, S., Morgenstern, O., Salawitch, R., Sofieva, V., Tourpali, K., Tweedy, O., Zawada, D., Steinbrecht, W., and Weber, M.: Chapter 3: Update on Global Ozone: Past, Present, and Future, in Scientific Assessment of Ozone Depletion 2018, World Meteorological Organization, Global Ozone Research and Monitoring Global Ozone Research and Monitoring Project - Report No. 58, 1–78 pp., 2018.

Brioude, J., Portmann, R. W., Daniel, J. S., Cooper, O. R., Frost, G. J., Rosenlof, K. H., Granier, C., Ravishankara, A. R., Montzka, S. A., and Stohl, A.: Variations in ozone depletion potentials of very short-lived substances with season and emission region, Geophys. Res. Lett., 37, 1–5, https://doi.org/10.1029/2010GL044856, 2010.

Bühlmann, T., Garcia-Iturrate, M., Vollmer, M. K., Reiman, S., and Pascale, C.: METAS-2021: SI-traceable primary reference gas mixtures for HFC-32, HFC-365mfc, CH_2Cl_2, CCl_4, 1,2-dichloroethane and HFO-1336mzz(Z) at atmospheric amount-of-substance fractions (in preparation), n.d.

Burkholder, J. B., Sander, S. P., Abbatt, J. P. D., Barker, J. R., Cappa, C., Crounse, J. D., Dibble, T. S., Huie, R. E., Kolb, C. E., Kurylo, M. J., Orkin, V. L., Percival, C. J., Wilmouth, D. M., and Wine, P. H.: Chemical kinetics and photochemical data for use in atmospheric studies; evaluation number 19. Available at: https://hdl.handle.net/2014/49199, 2020.

Burkholder, J. B., Hodnebrog, Ø., McDonald, B. C., Orkin, V., Papadimitriou, V. C., and Van Hoomissen, D.: Annex: Summary of Abundances, Lifetimes, ODPs, REs, GWPs, and GTPs, in Scientific Assessment of Ozone Depletion 2022, World Meteorological Organization, Global Ozone Research and Monitoring - GAW Report No. 278, 1–58 pp., 2022.

Carpenter, L. J., Reimann, S., Burkholder, J. B., Clerbaux, C., Hall, B. D., Hossaini, R., Laube, J. C., and Yvon-Lewis, S. A.: Chapter 1: Update on Ozone-Depleting Substances (ODSs) and Other Gases of Interest to the Montreal Protocol, in Scientific Assessment of Ozone Depletion 2014, World Meteorological Organization, Global Ozone Research and Monitoring Project - Report No. 55, World Meteorological Organization, 1–105 pp., 2014.

CEH: Ethylene Dichloride, https://www.spglobal.com/commodity-insights/en/products-solutions/chemicals/chemical-economics-handbooks-ceh, last access 31 October 2025, https://doi.org/10.1021/cen-v033n039.p4084, 2025.

Chipperfield, M. P., Hossaini, R., Montzka, S. A., Reimann, S., Sherry, D., and Tegtmeier, S.: Renewed and emerging concerns over the production and emission of ozone-depleting substances, Nat. Rev. Earth Environ., 1, 251–263, https://doi.org/10.1038/s43017-020-0048-8, 2020.

Chipperfield, M. P., Santee, M. L., Alexander, S. P., de Laat, A. T. J., Kinnison, D. E., Kuttippurath, J., Langematz, U., Wargan, K., Dhomse, S. S., Grooß, J.-U., Keeble, J., Lawrence, Z. D., Manney, G. L., Müller, R., Nash, E., Newman, P. A., Plummer, D. A., Safieddine, S., Tritscher, I., von der Gathen, P., Weber, M., Wohltmann, I., Solomon, S., and Weber, M.: Chapter 4: Polar Stratospheric Ozone: Past, Present, and Future, in Scientific Assessment of Ozone Depletion 2022, World Meteorological Organization, Global Ozone Research and Monitoring - GAW Report No. 278, 1–55 pp., 2022.

Claxton, T., Hossaini, R., Wild, O., Chipperfield, M. P., and Wilson, C.: On the Regional and Seasonal Ozone Depletion Potential of Chlorinated Very Short-Lived Substances, Geophys. Res. Lett., 46, 5489–5498, https://doi.org/10.1029/2018GL081455, 2019.

Crawford, J. H., Ahn, J. Y., Al-Saadi, J., Chang, L., Emmons, L. K., Kim, J., Lee, G., Park, J. H., Park, R. J., Woo, J. H., Song, C. K., Hong, J. H., Hong, Y. D., Lefer, B. L., Lee, M., Lee, T., Kim, S., Min, K. E., Yum, S. S., Shin, H. J., Kim, Y. W., Choi, J. S., Park, J. S., Szykman, J. J., Long, R. W., Jordan, C. E., Simpson, I. J., Fried, A., Dibb, J. E., Cho, S. Y., and Kim, Y. P.: The Korea-United States air quality (KORUS-AQ) field study, Elementa, 9, 1–27, https://doi.org/10.1525/elementa.2020.00163, 2021.

Cunnold, D. M., Prinn, R. G., Rasmussen, R. A., Simmonds, P. G., Alyea, F. N., Cardelino, C. A., Crawford, A. J., Fraser, P. J., and Rosen, R. D.: The Atmospheric Lifetime Experiment: 3. Lifetime Methodology and Application to Three Years of $CFCl_3$ Data, J. Geophys. Res., 88, 8379–8400, 1983.

Daniel, J. S., Reimann, S., Ashford, P., Fleming, E. L., Hossaini, R., Lickley, M. J., Schofield, R., Walter-Terrinoni, H., McBride, L., Park, S., Ross, M. N., Salawitch, R. J., Sherry, D., Tegtmeier, S., Velders, G. J. M., Kuijpers, L. J. M., and Wuebbles, D. J.: Chapter 7: Scenarios and Information for Policymakers, in Scientific Assessment of Ozone Depletion 2022, World Meteorological Organization, Global Ozone Research and Monitoring - GAW Report No. 278, 1–50 pp., 2022.

DEFRA: UK Department for Environment, Food & Rural Affairs: https://www.gov.uk/guidance/uk-pollutant-release-and-transfer-register-prtr-data-sets, last access 15 January 2026, 2012.

Dubé, K., Saunders, L. N., Tegtmeier, S., Bourassa, A., Laube, J. C., Engel, A., Walker, K. A., Hossaini, R., and Bednarz, E. M.: Chlorinated very short-lived substances offset the long-term reduction of inorganic stratospheric chlorine, Commun. Earth Environ., 6, 1–7, 2025.

ECHA: Background document for 1,2-dichloroethane, https://echa.europa.eu/documents/10162/c667ff11-b443-3d98-daf9-d6d77727bee1, last access 31 October 2025, 2012.

ECHA: European Chemicals Agency: ANNEX XV REPORT AN ASSESSMENT OF WHETHER THE USE OF 1,2-DICHLOROETHANE (EDC) IN ARTICLES SHOULD BE RESTRICTED IN ACCORDANCE WITH ARTICLE 69(2) OF REACH, 2022.

EEA: European Environment Agency: https://www.eea.europa.eu/en/datahub/datahubitem-view/9405f714-8015-4b5b-a63c-280b82861b3d, last access 15 January 2026, 2026.

Engel, A., Rigby, M., Burkholder, J. B., Fernandez, R. P., Froidevaux, L., Hall, B. D., Hossaini, R., Saito, T., Vollmer, M. K., and Yao, B.: Chapter 1: Update on Ozone-Depleting Substances (ODSs) and Other Gases of Interest to the Montreal Protocol, in Scientific Assessment of Ozone Depletion 2018, World Meteorological Organization, Global Ozone Research and Monitoring Project - Report No. 58, 1–91 pp., 2018.

EPA: Environmental Protection Agency: Use Report for 1,2-Dichloroethane, 1–74 pp., 2020a.

EPA: United States Environmental Protection Agency: Final Scope of the Risk Evaluation for 1,2-Dichloroethane, CASRN 107-06-2, 2020b.

EPA: United States Environmental Protection Agency: Draft Human Health Hazard Assessment for 1,2-Dichloroethane: Technical Support Document for the Draft Risk Evaluation, CASRN 107-06-2, 1–171, 2024.

EPA: Environmental Protection Agency: Chemical Data Reporting under the Toxic Substances Control Act, https://www.epa.gov/chemical-data-reporting, last access 17 December 2025, 2025a.

EPA: Environmental Protection Agency: https://www.epa.gov/chemical-data-reporting/access-chemical-data-reporting-data, last access 30 September 2025, 2025b.

EPA: ENVIRONMENTAL PROTECTION AGENCY: Federal 1,2-Dichloroethane; Final Risk Evaluation Under the Toxic Substances Control Act (TSCA); Notice of Availability, 2026.

Feng, L., Smith, S. J., Braun, C., Crippa, M., Gidden, M. J., Hoesly, R., Klimont, Z., Van Marle, M., Van Den Berg, M., and Van Der Werf, G. R.: The generation of gridded emissions data for CMIP6, Geosci. Model Dev., 13, 461–482, https://doi.org/10.5194/gmd-13-461-2020, 2020.

Ganesan, A. L., Rigby, M., Zammit-Mangion, A., Manning, A. J., Prinn, R. G., Fraser, P. J., Harth, C. M., Kim, K. R., Krummel, P. B., Li, S., Mühle, J., O'Doherty, S. J., Park, S., Salameh, P. K., Steele, L. P., and Weiss, R. F.: Characterization of uncertainties in atmospheric trace gas inversions using hierarchical Bayesian methods, Atmos. Chem. Phys., 14, 3855–3864, https://doi.org/10.5194/acp-14-3855-2014, 2014.

GCWerks: https://www.gcwerks.com/, last access 12 February 2026, 2026.

Guillevic, M., Vollmer, M. K., Wyss, S. A., Leuenberger, D., Ackermann, A., Pascale, C., Niederhauser, B., and Reimann, S.: Dynamic-gravimetric preparation of metrologically traceable primary calibration standards for halogenated greenhouse gases, Atmos. Meas. Tech., 11, 3351–3372, https://doi.org/10.5194/amt-11-3351-2018, 2018.

Hall, B. D., Dutton, G. S., and Elkins, J. W.: The NOAA nitrous oxide standard scale for atmospheric observations, J. Geophys. Res. Atmos., 112, 1–9, https://doi.org/10.1029/2006JD007954, 2007.

Henne, S., Brunner, D., Oney, B., Leuenberger, M., Eugster, W., Bamberger, I., Meinhardt, F., Steinbacher, M., and Emmenegger, L.: Validation of the Swiss methane emission inventory by atmospheric observations and inverse modelling, Atmos. Chem. Phys., 16, 3683–3710, https://doi.org/10.5194/acp-16-3683-2016, 2016.

Hodnebrog, Aamaas, B., Fuglestvedt, J. S., Marston, G., Myhre, G., Nielsen, C. J., Sandstad, M., Shine, K. P., and Wallington, T. J.: Updated Global Warming Potentials and Radiative Efficiencies of Halocarbons and Other Weak Atmospheric Absorbers, Rev. Geophys., 58, 1–30, https://doi.org/10.1029/2019RG000691, 2020.

Hossaini, R., Chipperfield, M. P., Montzka, S. A., Rap, A., Dhomse, S., and Feng, W.: Efficiency of short-lived halogens at influencing climate through depletion of stratospheric ozone, Nat. Geosci., 8, 186–190, https://doi.org/10.1038/ngeo2363, 2015.

Hossaini, R., Atlas, E., Dhomse, S. S., Chipperfield, M. P., Bernath, P. F., Fernando, A. M., Mühle, J., Leeson, A. A., Montzka, S. A., Feng, W., Harrison, J. J., Krummel, P., Vollmer, M. K., Reimann, S., O'Doherty, S., Young, D., Maione, M., Arduini, J., and Lunder, C. R.: Recent Trends in Stratospheric Chlorine From Very Short-Lived Substances, J. Geophys. Res. Atmos., 124, 2318–2335, https://doi.org/10.1029/2018JD029400, 2019.

Hossaini, R., Sherry, D., Wang, Z., Chipperfield, M. P., Feng, W., Oram, D. E., Adcock, K. E., Montzka, S. A., Simpson, I. J., Mazzeo, A., Leeson, A. A., Atlas, E., and Chou, C. C. K.: On the atmospheric budget of 1,2-dichloroethane and its impact on stratospheric chlorine and ozone (2002-2020), Atmos. Chem. Phys., 24, 13457–13475, https://doi.org/10.5194/acp-24-13457-2024, 2024.

Jesswein, M., Lauther, V., Emig, N., Hoor, P., Keber, T., Lachnitt, H.-C., Ort, L., Schuck, T., Strobel, J., Van Luijt, R., Volk, C. M., Weyland, F., and Engel, A.: Tracing elevated abundance of CH_2Cl_2 in the subarctic upper troposphere to the Asian Summer Monsoon, Atmos. Chem. Phys., 25, 8107–8126, https://doi.org/doi.org/10.5194/acp-25-8107-2025, 2025.

Jones, A., Thomson, D., Hort, M., and Devenish, B.: The U.K. Met Office's Next-Generation Atmospheric Dispersion Model, NAME III, in: Air Pollution Modeling and its Application XVII, 17th ed., edited by: Borrego, C. and Norman, A.-L., Springer, New York, 580–589 pp., 2007.

Katharopoulos, I., Rust, D., Vollmer, M. K., Reimann, S., Doherty, J. O., Young, D., Stanley, K. M., Brunner, D.,

Emmenegger, L., and Henne, S.: Impact of transport model resolution and a-priori assumptions on inverse modeling of Swiss F-gases emissions, Atmos. Chem. Phys., 23, 14159–14186, https://doi.org/submitted, 2023.

Langenfelds, R. L., Fraser, P. J., Francey, R. J., Steele, L. P., Porter, L. W., and Allison, C. E.: The Cape Grim Air Archive: The first seventeen years, 1978 - 1995, in: Baseline Atmospheric Program Australia 1994 - 95, edited by: Francey, R. J., Dick, A. L., and Derek, N., 53–70, 1996.

Laube, J. C., Engel, A., Bönisch, H., Möbius, T., Worton, D. R., Sturges, W. T., Grunow, K., and Schmidt, U.: Contribution of very short-lived organic substances to stratospheric chlorine and bromine in the tropics – a case study, Atmos. Chem. Phys., 8, 7325–7334, https://doi.org/10.5194/acp-8-7325-2008, 2008.

Laube, J. C., Tegtmeier, S., Fernandez, R. P., Harrison, J., Hu, L., Krummel, P., Mahieu, E., Park, S., Western, L., Atlas, E., Bernath, P., Cuevas, C. A., Dutton, G., Froidevaux, L., Hossaini, R., Keber, T., Koenig, T. K., Montzka, S. A., Mühle, J., O'Doherty, S., Oram, D. E., Pfeilsticker, K., Prignon, M., Quack, B., Rigby, M., Rotermund, M., Saito, T., Simpson, I. J., Smale, D., Vollmer, M. K., Young, D., Engel, A., and Yao, B.: Chapter 1: Update on Ozone-Depleting Substances (ODSs) and Other Gases of Interest to the Montreal Protocol, in Scientific Assessment of Ozone Depletion 2022, World Meteorological Organization, Global Ozone Research and Monitoring - GAW Report No. 278, 1–63 pp., 2022.

Lauther, V., Vogel, B., Wintel, J., Rau, A., Hoor, P., Bense, V., Müller, R., and Volk, C. M.: In situ observations of CH_2Cl_2 and $CHCl_3$ show efficient transport pathways for very short-lived species into the lower stratosphere via the Asian and the North American summer monsoon, Atmos. Chem. Phys., 22, 2049–2077, https://doi.org/10.5194/acp-22-2049-2022, 2022.

Law, K., Sturges, W. T., Blake, D. R., Bake, N. J., Burkholder, J. B., Butler, J. H., Cox, R. A., Haynes, P. H., Ko, M. K. ., Kreher, K., Mari, C., Pfeilsticker, K., Plane, J. M. C., Salawitch, R. J., Schiller, C., Sinnhuber, B.-M., Von Glasow, R., Warwick, N. J., Wuebbles, D. J., and Yvon-Lewis, S. A.: Chapter 2: Halogenated Very Short-Lived Substances, in Scientific Assessment of Ozone Depletion 2006, World Meteorological Organization, Global Ozone Research and Monitoring - Report No. 50, 1–61 pp., 2006.

Liang, Q., Newman, P. A., Fleming, E. L., Lait, L. R., Atlas, E., Pan, L., Kinnison, D., Western, L. M., Schauffler, S., Smith, K., Treadaway, V., Hendershot, R., Donnelly, S., and Lueb, R.: Asian Summer Monsoon Anticyclone—The Primary Entryway for Chlorinated Very-Short-Lived Substances to the Stratosphere, Geophys. Res. Lett., 52, 1–10, https://doi.org/10.1029/2024GL110248, 2025.

Logue, J. M., Small, M. J., Stern, D., Maranche, J., and Robinson, A. L.: Spatial variation in ambient air toxics concentrations and health risks between industrial-influenced, urban, and rural sites, J. Air Waste Manag. Assoc., 60, 271–286, https://doi.org/10.3155/1047-3289.60.3.271, 2010.

Lyu, X., Guo, H., Wang, Y., Zhang, F., Nie, K., Dang, J., Liang, Z., Dong, S., Zeren, Y., Zhou, B., Gao, W., Zhao, S., and Zhang, G.: Hazardous volatile organic compounds in ambient air of China, Chemosphere, 246, 125731, https://doi.org/10.1016/j.chemosphere.2019.125731, 2020.

Maione, M., Giostra, U., Arduini, J., Furlani, F., Graziosi, F., Vullo, E. Lo, and Bonasoni, P.: Ten years of continuous observations of stratospheric ozone depleting gases at Monte Cimone (Italy) — Comments on the effectiveness of the Montreal

Protocol from a regional perspective, Sci. Total Environ., 446, 155–164, 2013.

Manning, A. J., Redington, A. L., Say, D., Doherty, S. O., Young, D., Simmonds, P. G., Vollmer, M. K., Mühle, J., Arduini, J., Spain, G., Wisher, A., Maione, M., Schuck, T. J., Stanley, K., Reimann, S., Engel, A., Krummel, B., Fraser, P. J., Harth, C. M., Salameh, P. K., Weiss, R. F., Gluckman, R., Brown, P. N., Watterson, J. D., and Arnold, T.: Evidence of a recent decline in UK emissions of hydrofluorocarbons determined by the InTEM inverse model and atmospheric measurements, Atmos. Chem. Phys., 12739–12755, https://doi.org/10.5194/acp-21-12739-2021, 2021.

Mao, T., Wang, Y., Xu, H., Jiang, J., Wu, F., and Xu, X.: A study of the atmospheric VOCs of Mount Tai in June 2006, Atmos. Environ., 43, 2503–2508, https://doi.org/10.1016/j.atmosenv.2009.02.013, 2009.

MassBank: https://massbank.eu/MassBank/RecordDisplay?id=MSBNK-Fac_Eng_Univ_Tokyo-JP000954, last access 19 December 2025, 2025.

MCgroup: Merchant Research & Consulting ltd: Ethylene Dichloride: Role in the Modern Chemical Landscape & Market Insights, Ethylene Dichloride: Role in the Modern Chemical Landscape & Market Insights, last access 10 November 2025, 2023.

Miller, B. R., Weiss, R. F., Salameh, P. K., Tanhua, T., Greally, B. R., Mühle, J., and Simmonds, P. G.: Medusa: A Sample Preconcentration and GC/MS Detector System for in Situ Measurements of Atmospheric Trace Halocarbons, Hydrocarbons, and Sulfur Compounds, Anal. Chem., 80, 1536–1545, https://doi.org/10.1021/ac702084k, 2008.

Montzka, S. A., Dutton, G. S., Yu, P., Ray, E., Portmann, R. W., Daniel, J. S., Kuijpers, L., Hall, B. D., Mondeel, D., Siso, C., Nance, D. J., Rigby, M., Manning, A. J., Hu, L., Moore, F., Miller, B. R., and Elkins, J. W.: An unexpected and persistent increase in global emissions of ozone-depleting CFC-11, Nature, 557, 413–417, 2018.

NASA: Korea United States Air Quality Study, EarthData, https://doi.org/10.5067/Suborbital/KORUSAQ/DATA01, 2024.

NIST: https://webbook.nist.gov/cgi/cbook.cgi?ID=C107062&Mask=200#Mass-Spec, last access 19 December 2025, 2026.

NOAA: https://www.esrl.noaa.gov/gmd/hats/, last access 6 June 2025, 2025.

Oram, D. E., Ashfold, M. J., Laube, J. C., Gooch, L. J., Humphrey, S., Sturges, W. T., Leedham-Elvidge, E., Forster, G. L., Harris, N. R. P., Mead, M. I., Samah, A. A., Phang, S. M., Ou-Yang, C.-F., Lin, N.-H., Wang, J.-L., Baker, A. K., Brenninkmeijer, C. A. M., and Sherry, D.: A growing threat to the ozone layer from short-lived anthropogenic chlorocarbons, Atmos. Chem. Phys., 17, 11929–11941, 2017.

Pan, L. L., Atlas, E. L., Honomichl, S. B., Smith, W. P., Kinnison, D. E., Solomon, S., Santee, M. L., Saiz-Lopez, A., Laube, J. C., Wang, B., Ueyama, R., Bresch, J. F., Hornbrook, R. S., Apel, E. C., Hills, A. J., Treadaway, V., Smith, K., Schauffler, S., Donnelly, S., Hendershot, R., Lueb, R., Campos, T., Viciani, S., D'Amato, F., Bianchini, G., Barucci, M., Podolske, J. R., Iraci, L. T., Gurganus, C., Bui, P., Dean-Day, J. M., Millán, L., Ryoo, J.-M., Barletta, B., Koo, J.-H., Kim, J., Liang, Q., Randel, W. J., Thornberry, T., and Newman, P. A.: East Asian summer monsoon delivers large abundances of very short-lived organic chlorine substances to the lower stratosphere, Proc. Natl. Acad. Sci., 121, 1–10, https://doi.org/10.1073/pnas., 2024.

Pisso, I., Haynes, P. H., and Law, K. S.: Emission location dependent ozone depletion potentials for very short-lived halogenated species, Atmos. Chem. Phys., 10, 12025–12036, https://doi.org/10.5194/acp-10-12025-2010, 2010.

Prinn, R. G., Weiss, R. F., Fraser, P. J., Simmonds, P. G., Cunnold, D. M., Alyea, F. N., O'Doherty, S., Salameh, P., Miller, B. R., Huang, J., Wang, R. H. J., Hartley, D. E., Harth, C., Steele, L. P., Sturrock, G., Midgley, P. M., and McCulloch, A.: A history of chemically and radiatively important gases in air deduced from ALE/GAGE/AGAGE, J. Geophys. Res., 105, 17751–17792, https://doi.org/10.1029/2000JD900141, 2000.

Prinn, R. G., Weiss, R. F., Arduini, J., Arnold, T., Langley DeWitt, H., Fraser, P. J., Ganesan, A. L., Gasore, J., Harth, C. M., Hermansen, O., Kim, J., Krummel, P. B., Li, S., Loh, Z. M., Lunder, C. R., Maione, M., Manning, A. J., Miller, B. R., Mitrevski, B., Mühle, J., O'Doherty, S., Park, S., Reimann, S., Rigby, M., Saito, T., Salameh, P. K., Schmidt, R., Simmonds, P. G., Paul Steele, L., Vollmer, M. K., Wang, R. H., Yao, B., Yokouchi, Y., Young, D., and Zhou, L.: History of chemically and radiatively important atmospheric gases from the Advanced Global Atmospheric Gases Experiment (AGAGE), Earth Syst. Sci. Data, 10, 985–1018, https://doi.org/10.5194/essd-10-985-2018, 2018.

Ramsden, A., Danjou, A., de Longueville, H., Melo, D. B., Constantin, L., Thanwerdas, J., Henne, S., and Bruch, V.: Flux Intercomparison Environment (FLUXIE) [Code], https://github.com/openghg/fluxie, 2025.

Reimann, S., Western, L. M., Lickley, M. J., Sherry, D., Daniel, J. S., Kuijpers, L. J. M., Montzka, S. A., Rigby, M., Velders, G. J. M., Vollmer, M. K., Emmenegger, L., Liang, Q., Park, S., and Solomon, S.: Continuing industrial emissions are delaying the recovery of the stratospheric ozone layer, Nat. Commun., 13–20, https://doi.org/10.1038/s41467-026-70533-w, 2026.

Rigby, M. and Western: mrghg/py12box_invert: v0.0.2 [Code], https://doi.org/https://doi.org/10.5281/zenodo.6857794, 2022a.

Rigby, M. and Western, L.: mrghg/py12box: v0.2.2 [Code], https://doi.org/https://doi.org/10.5281/zenodo.6868589, 2022b.

Rigby, M., Prinn, R. G., O'Doherty, S., Miller, B. R., Ivy, D., Mühle, J., Harth, C. M., Salameh, P. K., Arnold, T., Weiss, R. F., Krummel, P. B., Steele, L. P., Fraser, P. J., Young, D., and Simmonds, P. G.: Recent and future trends in synthetic greenhouse gas radiative forcing, Geophys. Res. Lett., 41, 2623–2630, https://doi.org/10.1002/2013GL059099, 2014.

Roozitalab, B., Emmons, L. K., Hornbrook, R. S., Kinnison, D. E., Fernandez, R. P., Li, Q., Saiz-lopez, A., Hossaini, R., Cuevas, C. A., and Apel, E. C.: Measurements and Modeling of the Interhemispheric Differences of Atmospheric Chlorinated Very Short-Lived Substances Journal of Geophysical Research : Atmospheres, 1–27, https://doi.org/10.1029/2023JD039518, 2024.

Ruckstuhl, A. F., Henne, S., Reimann, S., Steinbacher, M., Vollmer, M. K., O'Doherty, S., Buchmann, B., and Hueglin, C.: Robust extraction of baseline signal of atmospheric trace species using local regression, Atmos. Meas. Tech., 5, 2613–2624, https://doi.org/10.5194/amt-5-2613-2012, 2012.

Savitzky, A. and Golay, M. J. E.: Smoothing and Differentiation of Data by Simplified Least Squares Procedures, Anal. Chem., 36, 1627–1639, 1964.

Sherwood, J.: European Restrictions on 1,2-Dichloroethane: C-H Activation Research and Development Should Be Liberated and not Limited, Angew. Chemie Int. Ed., 57, 14286–14290, https://doi.org/10.1002/anie.201800549, 2018.

Simpson, I. J., Blake, D. R., Blake, N. J., Meinardi, S., Barletta, B., Hughes, S. C., Fleming, L. T., Crawford, J. H., Diskin, G. S., Emmons, L. K., Fried, A., Guo, H., Peterson, D. A., Wisthaler, A., Woo, J. H., Barré, J., Gaubert, B., Kim, J., Kim, M. J.,

Kim, Y., Knote, C., Mikoviny, T., Pusede, S. E., Schroeder, J. R., Wang, Y., Wennberg, P. O., and Zeng, L.: Characterization, sources and reactivity of volatile organic compounds (VOCs) in Seoul and surrounding regions during KORUS-AQ, Elementa, 8, https://doi.org/10.1525/elementa.434, 2020.

Statista: Production capacity of ethylene dichloride worldwide in 2018 and 2023, https://www.statista.com/statistics/1063227/global-ethylene-dichloride-production-capacity/, last access 10 November 2025, 2023.

Sutherland, I. W., Hamilton, N. G., Dudman, C. C., Jones, P., Lennon, D., and Winfield, J. M.: General Chlorination and dehydrochlorination reactions relevant to the manufacture of trichloroethene and tetrachloroethene Part 1. Reaction pathways, Appl. Catal. A Gen., 399, 1–11, https://doi.org/10.1016/j.apcata.2011.02.035, 2011.

Takahashi, L., Yamada, T., Okamoto, H., and Takahashi, K.: Unveiling the relation between multiple chemical products and process conditions for trichloroethylene and perchloroethylene production via catalysis network analysis, Catal. Sci. Technol., 14, 4927–4938, https://doi.org/10.1039/d4cy00573b, 2024.

TEAP: Report of the Technology and Economic Assessment Panel, Volume 1: Progress Report, 2024.

Thompson, C. R., Wofsy, S. C., Prather, M. J., Newman, P. A., Hanisco, T. F., Ryerson, T. B., Fahey, D. W., Apel, E. C., Brock, C. A., Brune, W. H., Froyd, K., Katich, J. M., Nicely, J. M., Peischl, J., Ray, E., Veres, P. R., Wang, S., Allen, H. M., Asher, E., Bian, H., Blake, D., Bourgeois, I., Budney, J., Paul Bui, T., Butler, A., Campuzano-Jost, P., Chang, C., Chin, M., Commane, R., Correa, G., Crounse, J. D., Daube, B., Dibb, J. E., DiGangi, J. P., Diskin, G. S., Dollner, M., Elkins, J. W., Fiore, A. M., Flynn, C. M., Guo, H., Hall, S. R., Hannun, R. A., Hills, A., Hintsa, E. J., Hodzic, A., Hornbrook, R. S., Greg Huey, L., Jimenez, J. L., Keeling, R. F., Kim, M. J., Kupc, A., Lacey, F., Lait, L. R., Lamarque, J. F., Liu, J., McKain, K., Meinardi, S., Miller, D. O., Montzka, S. A., Moore, F. L., Morgan, E. J., Murphy, D. M., Murray, L. T., Nault, B. A., Andrew Neuman, J., Nguyen, L., Gonzalez, Y., Rollins, A., Rosenlof, K., Sargent, M., Schill, G., Schwarz, J. P., St. Clair, J. M., Steenrod, S. D., Stephens, B. B., Strahan, S. E., Strode, S. A., Sweeney, C., Thames, A. B., Ullmann, K., Wagner, N., Weber, R., Weinzierl, B., Wennberg, P. O., Williamson, C. J., Wolfe, G. M., and Zeng, L.: The NASA Atmospheric Tomography (ATom) Mission: Imaging the Chemistry of the Global Atmosphere, Bull. Am. Meteorol. Soc., 103, E761–E790, https://doi.org/10.1175/BAMS-D-20-0315.1, 2022.

Thompson, R. L. and Stohl, A.: FLEXINVERT: an atmospheric Bayesian inversion framework for determining surface fluxes of trace species using an optimized grid, Geosci. Model Dev., 7, 2223–2242, https://doi.org/10.5194/gmd-7-2223-2014, 2014.

UNEP: 1,2-DICHLOROETHANE, SIDS Initial Assessment Report for 14th SIAM, https://hpvchemicals.oecd.org/ui/handler.axd?id=95f8d194-732a-4cc9-b59b-839ed3b18732, last access 31 October 2025, 2002.

UNEP: Medical and Technical Options Committee (MCTOC) 2018 Assessment Report, 1–182 pp., 2018.

UNEP: Medical and Technical Options Committee (MCTOC) 2022 Assessment Report, United Nations Environment Programme, Nairobi, 1–329 pp., 2022.

Villamayor, J., Iglesias-Suarez, F., Cuevas, C. A., Fernandez, R. P., Li, Q., Abalos, M., Hossaini, R., Chipperfield, M. P.,

Kinnison, D. E., Tilmes, S., Lamarque, J. F., and Saiz-Lopez, A.: Very short-lived halogens amplify ozone depletion trends in the tropical lower stratosphere, Nat. Clim. Chang., 13, 554–560, https://doi.org/10.1038/s41558-023-01671-y, 2023.

Vollmer, M. K., Miller, B. R., Rigby, M., Reimann, S., Mühle, J., Krummel, P. B., O'Doherty, S., Kim, J., Rhee, T. S., Weiss, R. F., Fraser, P. J., Simmonds, P. G., Salameh, P. K., Harth, C. M., Wang, R. H. J., Steele, L. P., Young, D., Lunder, C. R., Hermansen, O., Ivy, D., Arnold, T., Schmidbauer, N., Kim, K. R., Greally, B. R., Hill, M., Leist, M., Wenger, A., and Prinn, R. G.: Atmospheric histories and global emissions of the anthropogenic hydrofluorocarbons HFC-365mfc, HFC-245fa, HFC-227ea, and HFC-236fa, J. Geophys. Res., 116, 1–16, https://doi.org/10.1029/2010JD015309, 2011.

Vollmer, M. K., Young, D., Trudinger, C. M., Mühle, J., Henne, S., Rigby, M., Park, S., Li, S., Guillevic, M., Mitrevski, B., Harth, C. M., Miller, B. R., Reimann, S., Yao, B., Steele, L. P., Wyss, S. A., Lunder, C. R., Arduini, J., McCulloch, A., Wu, S., Rhee, T. S., Wang, R. H. J., Salameh, P. K., Hermansen, O., Hill, M., Langenfelds, R. L., Ivy, D., O'Doherty, S., Krummel, P. B., Maione, M., Etheridge, D. M., Zhou, L., Fraser, P. J., Prinn, R. G., Weiss, R. F., and Simmonds, P. G.: Atmospheric histories and emissions of chlorofluorocarbons CFC-13 ($CClF_3$), ∑CFC-114 ($C_2Cl_2F_4$), and CFC-115 (C_2ClF_5), Atmos. Chem. Phys., 18, 979–1002, https://doi.org/10.5194/acp-18-979-2018, 2018.

Vollmer, M. K., Pitt, J. R., Young, D., Henne, S., Mitrevski, B., Mühle, J., Ganesan, A., Arduini, J., Manning, A. J., Wagenhäuser, T., Redington, A. L., Murphy, B., Gluckmann, R., Stanley, K. M., Krummel, P. B., Lunder, C. R., Yun, J., Rust, D., Wenger, A., Guillevic, M., Kim, J., Wang, R. H. J., Rhee, T. S., Constantin, L., Frumau, A., Harth, C. M., Salameh, P. K., Hermansen, O., Engel, A., Doherty, S. O., Park, S., Maione, M., Fraser, J., Prinn, R. G., Weiss, R. F., and Reimann, S.: Global Observations and European emissions of the halogenated olefins HFO-1234yf, HFO-1234ze(E), and HCFO-1233zd(E) from the AGAGE (Advanced Global Atmospheric Gases Experiment) network, Atmos. Chem. Phys., 26, 6993–7012, https://doi.org/10.5194/acp-26-6993-2026, 2026.

Western, L. M., Rigby, M., Mühle, J., Krummel, P. B., Lunder, C. R., Doherty, S. O., Reimann, S., Vollmer, M. K., Young, D., Adam, B., Fraser, P. J., Ganesan, A. L., Harth, C. M., Hermansen, O., Kim, J., Langenfelds, R. L., Loh, Z. M., Mitrevski, B., Pitt, J. R., Salameh, P. K., Schmidt, R., Stanley, K., Stavert, A. R., Wang, H., Weiss, R. F., and Prinn, R. G.: Global emissions and abundances of chemically and radiatively important trace gases from the AGAGE network, Earth Syst. Sci. Data, 17, 6557–6582, https://doi.org/https://doi.org/10.5194/essd-17-6557-2025, 2025.

WHO: ILO-WHO International Chemical Safety Cards (ICSCs); https://chemicalsafety.ilo.org/dyn/icsc/showcard.display?p_version=2&p_card_id=0250 ILO-WHO International Chemical Safety Cards (ICSCs), last access 14 May 2025, 2013.

Wofsy, S. C.: HIAPER Pole-to-Pole Observations (HIPPO): Fine-grained, global-scale measurements of climatically important atmospheric gases and aerosols, Philos. Trans. R. Soc. A Math. Phys. Eng. Sci., 369, 2073–2086, https://doi.org/10.1098/rsta.2010.0313, 2011.

Wofsy, S. C., Daube, B., Jimenez-Pizarro, R., Kort, E., Pittman, J. V., Park, S., Commane, R., Xiang, B., Santoni, G., Jacob, D. J., Fisher, J. A., Pickett-Heaps, C. A., Wang, H., Wecht, K. J., Wang, Q., Stephens, B. B., Shertz, S. R., Watt, A., Romashkin, M. J., Campos, T., Haggerty, J., Cooper, W. A., Rogers, D. C., Beaton, S., Hendershot, R., Elkins, J. W., Fahey, D. W., Gao,

R.-S., Schwarz, J. P., Moore, F., Montzka, S. A., Perring, A. E., Hurst, D., Miller, B. R., Sweeney, C., Oltmans, S. J., Hintsa, E. J., Nance, D., Dutton, G. S., Watts, L. A., Spackman, J. R., Rosenlof, K. H., Ray, E., Hall, B., Zondlo, M., Diao, M., Keeling, R. K., Bent, J., Atlas, E., Lueb, R., and Mahoney, M. J.: HIPPO Combined Discrete Flask and GC Sample GHG, Halocarbon, and Hydrocarbon Data, Version 1.0, UCAR/NCAR – Earth Observing Laboratory, https://doi.org/10.3334/CDIAC/HIPPO_012, 2017.

Wofsy, S. C., Afshar, S., Allen, H. M., Apel, E. C., Asher, E. C., Barletta, B., Bent, J., Bian, H., Biggs, B. C., Blake, D. R., Blake, N., Bourgeois, I., Brock, C. A., Brune, W. H., Budney, J. W., Bui, T. P., Butler, A., Campuzano-Jost, P., Chang, C. S., Chin, M., Commane, R., Correa, G., Crounse, J., Cullis, D., Dabue, B. C., Day, D. A., Dean-Day, J. M., Dibb, J. E., DiGangi, J. P., Diskin, G. S., Dollner, M., Elkins, J. W., Erdesz, F., Fiore, A. M., Flynn, C. M., Froyd, K. D., Gesler, D. W., Hall, S. R., Hanisco, T. F., Hannun, R. A., Hills, A. J., Hintsa, E. J., Hoffman, A., Hornbrook, R. S., Huey, L. G., Hughes, S., Jimenez, J. L., Johnson, B. J., Katich, J. M., Keeling, R. F., Kim, M. J., Kupc, A., Lait, L. R., McKain, K., Mclaughlin, R. J., Meinardi, S., Miller, D. O., Montzka, S. A., Moore, F. L., Morgan, E. J., Murphy, D. M., Murray, L. T., Nault, B. A., Neuman, J. A., Newman, P. A., Nicely, J. M., Pan, X., Paplawsky, W., Peischl, J., Prather, M. J., Price, D. J., Ray, E. A., Reeves, J. M., Richardson, M., Rollins, A. W., Rosenlof, K. H., Ryerson, T. B., Scheuer, E., Schill, G. P., Schroder, J. C., Schwarz, J. P., St.Clair, J. M., Steenrod, S. D., Stephens, B. B., Strode, S. A., Sweeney, C., Tanner, D., Teng, A. P., Thames, A. B., Thompson, C. R., Ullmann, K., Veres, P. R., Wagner, N. L., Watt, A., Weber, R., Weinzierl, B. B., Wennberg, P. O., Williamson, C. J., Wilson, J. C., et al.: ATom: Merged Atmospheric Chemistry, Trace Gases, and Aerosols, Version 2, ORNL DAAC, https://doi.org/10.3334/ORNLDAAC/1925, 2021.

Wu, Y. and An, H.: Green Catalytic Synthesis of Ethylenediamine from Ethylene Glycol and Monoethanolamine: A Review, ACS Omega, 9, 18747−18756, https://doi.org/10.1021/acsomega.4c00709, 2024.

Xu, Z., Zou, Q., Jin, L., Shen, Y., Shen, J., Xu, B., Qu, F., and Zhang, F.: Characteristics and sources of ambient Volatile Organic Compounds (VOCs) at a regional background site, YRD region, China: Significant influence of solvent evaporation during hot months, Sci. Total Environ., 857, 159674, https://doi.org/10.1016/j.scitotenv.2022.159674, 2023.

Yang, M., Wang, Y., Chen, J., Li, H., and Li, Y.: Aromatic hydrocarbons and halocarbons at a mountaintop in Southern China, Aerosol Air Qual. Res., 16, 478–491, https://doi.org/10.4209/aaqr.2015.03.0197, 2016.

Yvon-Lewis, S. A. and Butler, J. H.: Effect of oceanic uptake on atmospheric lifetimes of selected trace gases, J. Geophys. Res., 107, ACH 1-1-ACH 1-9, https://doi.org/10.1029/2001JD001267, 2002.

Zhang, J., Sun, Y., Wu, F., Sun, J., and Wang, Y.: The characteristics, seasonal variation and source apportionment of VOCs at Gongga Mountain, China, Atmos. Environ., 88, 297–305, https://doi.org/10.1016/j.atmosenv.2013.03.036, 2014.

Appendix A: Characterisation of DCE

Table A1. Identifiers, chemical, physical and atmospheric properties of DCE.[a]

Identifiers, chemical and physical properties	
IUPAC name	1,2-dichloroethane
CAS number (WHO, 2013)	107-06-2
Chemical formula (WHO, 2013)	$ClCH_2CH_2Cl$ / $C_2H_4Cl_2$
Boiling Point (°C) (WHO, 2013)	83.5
Molecular mass (g mol^{-1}) (WHO, 2013)	98.96
Exact mass (g mol^{-1}) (MassBank, 2025)	97.96901
Atmospheric Properties	
Total lifetime (days) (Burkholder and Hodnebrog et al., 2022)	81.3 (41–555)
Average tropospheric lifetime (days) (Burkholder and Hodnebrog et al., 2022)	82.1
Radiative Efficiency (W m^{-2} ppb^{-1}) (Burkholder and Hodnebrog et al., 2022)[b]	8.64×10^{-3}
GWP (100 yr) (Burkholder and Hodnebrog et al., 2022)	1
GTP (100 yr) (Burkholder and Hodnebrog et al., 2022)	<1
ODP (Claxton et al., 2019)	0.0029–0.0119[c]

[a]Global warming potential (GWP) on a 100-year horizon, global temperature change potential (GTP) on a 100-year horizon, ozone-depletion potential (ODP), photochemical ozone creation potential (POCP). [b]With adjustments regarding stratospheric temperature, lifetime, low-frequency infrared absorption (Burkholder and Hodnebrog et al., 2022). [c]Highest in tropical (Southeast-)Asia, lowest in Europe (Claxton et al., 2019).

Appendix B: Measurement sites

Table B1. Summary of the measurement sites, locations, the networks/institutions that contributed the 1,2-dichloroethane (DCE) measurements, the used instruments and calibration scales, the regions for which the data were used for emissions modelling and the time periods for which DCE measurements were used in this study.

site	latitude	longitude	network/ institute	instrument	calibration scale	modelling region
Alert (ALT), Nunavut, Canada	82.5° N	62.5° W	NOAA	flask	NOAA-2003	Global
Zeppelin (ZEP), Svalbard, Norway	78.9° N	11.9° E	AGAGE	Medusa	METAS-2021	Global
Summit (SUM), Greenland	72.6° N	38.4° W	NOAA	flask	NOAA-2003	Global
Barrow (BRW), Alaska, USA	71.3° N	156.6° W	NOAA	flask	NOAA-2003	Global
Mace Head (MHD), Ireland	53.3° N	9.9° W	AGAGE, NOAA	Medusa, flask	METAS-2021 NOAA-2003	Global, Europe
Tacolneston (TAC), UK	52.5° N	1.1° E	AGAGE	Medusa	METAS-2021	Europe
Taunus (TOB), Germany	50.2° N	8.4° E	AGAGE	Medusa	METAS-2021	Europe
Jungfraujoch (JFJ), Switzerland	46.5° N	8.0° E	AGAGE	Medusa	METAS-2021	Global, Europe
Park Falls (LEF), Wisconsin, USA	45.9° N	90.3° W	NOAA	flask	NOAA-2003	Global
Monte Cimone (CMN), Italy	44.2° N	10.7° E	AGAGE	ADS/ Medusa	METAS-2021	Europe
Harvard Forest (HFM), Massachusetts, USA	42.5° N	72.2° W	NOAA	flask	NOAA-2003	Global
Trinidad Head (THD), California, USA	41.0° N	124.1° W	AGAGE, NOAA	Medusa, flask	METAS-2021 NOAA-2003	Global, West USA
Niwot Ridge (NWR), Colorado, USA	40.1° N	105.6° W	NOAA	flask	NOAA-2003	Global
Scripps Institution of Oceanography (SIO), San Diego, California, USA	32.9° N	117.3° W	AGAGE	Medusa	METAS-2021	West USA
Mauna Kea (MKO), Hawaii, USA	19.8° N	155.5° W	NOAA	flask	NOAA-2003	–
Cape Kumukahi (KUM), Hawaii, USA	19.6° N	154.9° W	NOAA	flask	NOAA-2003	Global
Mauna Loa (MLO), Hawaii, USA	19.5° N	155.6° W	NOAA	flask	NOAA-2003	Global
Ragged Point (RPB), Barbados	13.2° N	59.4° W	AGAGE, NOAA	Medusa, flask	METAS-2021 NOAA-2003	Global
Cape Matatula (SMO), American Samoa	14.2° S	170.6° W	AGAGE, NOAA	Medusa, flask	METAS-2021 NOAA-2003	Global
Kennaook/Cape Grim (CGO), Tasmania, Australia	40.7° S	144.7° E	AGAGE, NOAA	Medusa, flask	METAS-2021 NOAA-2003	Global
King Sejong Station (KSG), Antarctica	62.2° S	58.8° W	KOPRI[b]/ Empa[c]	flask (Medusa)	METAS-2021	–
Palmer Station (PSA), Antarctica	64.8° S	64.1° W	NOAA	flask	NOAA-2003	Global
South Pole (SPO), Antarctica	90.0° S	24.8° W	NOAA	flask	NOAA-2003	Global

[a]Commonwealth Scientific and Industrial Research Organisation (CSIRO). [b]Korea Polar Research Institute (KOPRI). [c]Swiss Federal Laboratories for Materials Science and Technology (Empa).

Appendix C: Sampling and analysis

Additional instrumentation

At CMN the first years of the DCE record is completed by measurements made using an Adsorption Desorption System (ADS) (Maione et al., 2013). In the first approximately 2 years, the sampling frequency was one ambient air and one working standard measurement every two hours (std_sample, air_sample, std_sample). Later, two ambient air measurements were bracketed by working standard measurements (std_sample, air_sample, air_sample, std_sample). Samples consisting of 1 L of air were trapped at −30 °C on a trap filled with four adsorbent materials (Carbograph 2TD, Carbograph 1TD, Carboxen 1000 and Carbosieve SIII), using a UNITY2-AirServer2 (Markes International, UK). The analytes were thermally desorbed onto a J&W GS-GasPro (0.32 mm ID x 30 m; Agilent) gas chromatographic column and detected by EI-MS (Agilent 6850–5975) in SIM mode. The measurements are made available in the GCWerks (GCWerks, 2026) software.

DCE peak identification and chromatography

Within AGAGE, DCE peak identification was achieved by a scan measurement of a diluted sample (MC-2019D) of a high-mole fraction trace gas mixture made of pure substances (Synquest Laboratories) on the Empa-Medusa-GC/MS system. In 40 mL of a sample at 6.17 ppb mole fraction (equivalent to 11 pmol), the ions listed in Table C1 (column 1), in units m/z, were detected at the indicated relative abundance (column 3). The scanned fragment ions ranged m/z 43–150. Fragment ions m/z 44 and 104 are identified as contamination in the carrier gas and/or column bleed and should be ignored. For detection on Medusa-GC/MS instruments, mass/charge (m/z) 62 ($[C_2H_3{}^{35}Cl]^+$) is used as the target mass. Qualifying masses used are m/z 98 ($[C_2H_4{}^{35}Cl_2]^+$), m/z 64 ($[C_2H_3{}^{37}Cl]^+$), or m/z 49 ($[CH_2{}^{35}Cl]^+$). Additional spectra from the literature are also shown in Table C1 (columns 1, 4, 5).

Chromatographic separation on the Medusa systems was achieved with a PoraBOND Q column (0.32 mm ID x 25 m; 5 µm film thickness; Agilent), resulting in fairly symmetric (sometimes slightly tailing) peaks with stable baseline at most sites and times. Depending on column age or column manipulation during maintenance, retention times of DCE varied, exhibiting increasing retention times with increasing column age. Therefore, 1400–1500 s is given as the approximate time range for elution. On the Medusa systems, DCE elutes between specific substances measured by the whole network, i.e. H-2402 (CF_2BrCF_2Br) and chloroform ($CHCl_3$) at lower retention times, and dibromo methane (CH_2Br_2) and benzene (C_6H_6) at higher retention times. Chromatograms are integrated by peak area and peak height but reported mole fractions are solely based on peak areas. An example chromatogram showing the target and qualifier ions is given in Fig. C1.

On the CMN ADS instrument, using a J&W GS-GasPro (0.32 mm ID x 30 m; Agilent) chromatographic column, benzene eluted on the tail of the DCE peak. Therefore, the reported mole fractions were calculated by integrating the chromatographic peaks by height.

Table C1. Mass spectra of DCE (1,2-dichloroethane, CH_2ClCH_2Cl). Intensities are given relative to m/z 62.

m/z	proposed fragment	relative intensity (%)		
		Medusa-GC/MS	NIST (2026)	MassBank (2025)
104	–	1.1	–	–
102	$C_2H_4{}^{37}Cl_2{}^+$	1.4	1.3	–
100	$C_2H_4{}^{35}Cl\,{}^{37}Cl^+$	8.2	5.1	4.5
98	$C_2H_4{}^{35}Cl_2{}^+$	12.8	8.5	7.3
65	$C_2H_4{}^{37}Cl^+$	4.4	3.4	0.32
64	$C_2H_3{}^{37}Cl^+$	32.8	33.3	31.1
63	$C_2H_4{}^{35}Cl^+$	16.8	14.5	12.5
62	$C_2H_3{}^{35}Cl^+$	100	100	99.99
61	$C_2H_2{}^{35}Cl^+$	10.5	13.2	0.88
60	$C_2H^{35}Cl^+$	3.2	4.7	3.2
59	$C_2{}^{35}Cl^+$	–	1.3	–
51	$CH_2{}^{37}Cl^+$	8.2	7.3	7.8
50	$CH^{37}Cl^+$	–	1.7	–
49	$CH_2{}^{35}Cl^+$	1.8	20.5	24.9
48	$CH^{35}Cl^+$	–	3.4	0.22
47	$C^{35}Cl^+$	–	3	2.1
44	–	1.6	–	–
38	$H^{37}Cl^+$	–	0.85	–
37	$^{37}Cl^+$	–	4.3	–
36	$H^{35}Cl^+$	–	2.1	2.6
35	$^{35}Cl^+$	–	4.7	4.2
32	–	–	1.7	–
28	$C_2H_4{}^+$	–	6.4	0.33
27	$C_2H_3{}^+$	–	20.9	39.8
26	$C_2H_2{}^+$	–	10.3	13.1
25	C_2H^+	–	3	3
14	$CH_2{}^+$	–	0.85	–

985

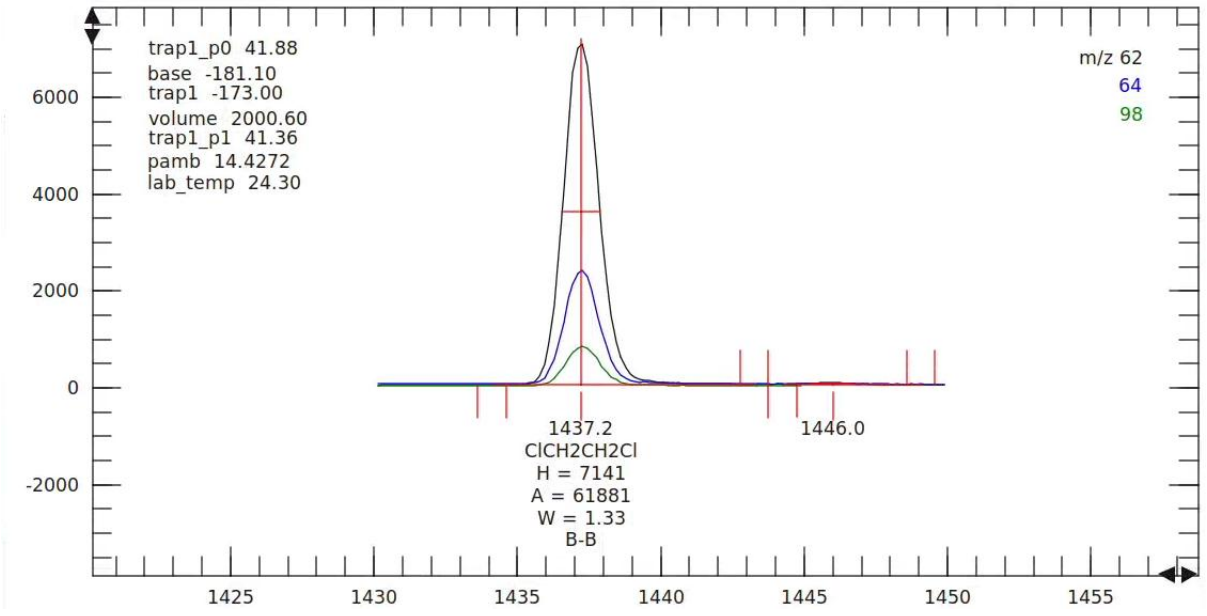

Figure C1. Example chromatogram of DCE, x-axis in seconds, y-axis in arbitrary units, from the analysis of 2 L of a working standard (18.7 ppt) with a Medusa-GC/MS instrument. The target ion with mass/charge (m/z) 62 (black line), and two qualifier ions with m/z 64 (blue line) and m/z 98 (green line) were detected at the retention time of 1437.2 s.

The identification of DCE on NOAA instruments was achieved by comparing the retention time and mass spectrum obtained from an analysis of a standard containing DCE on the M3 and M4 instruments to results from the analysis of ambient air. This procedure confirmed the peak identification and retention time, and monitoring m/z = 62 resulted in a peak without substantial obvious interferences in the majority of flask-air samples analysed at NOAA.

Appendix D: Monte Cimone instrument comparison (Medusa-ADS)

At CMN station, the old ADS and new Medusa systems were run in parallel for about 14 months to track the transition between the two set-ups. Both instruments used the same working standard tank (quaternary) and calibration tank (tertiary) for the regular calibration of measurements. Both systems sampled real air from the same main sampling line but flushed with their own pumping system. The timing of sampling for the two instruments was not perfectly synchronised due to different chromatographic configurations. The results of the comparison for the matching runs (within ± 20 min) are summarized below: timeseries (Fig. D1), orthogonal (Deming) regression scatterplot (Fig. D2), Blant–Alman plot of residuals (Fig. D3), and a statistics summary (Table D1).

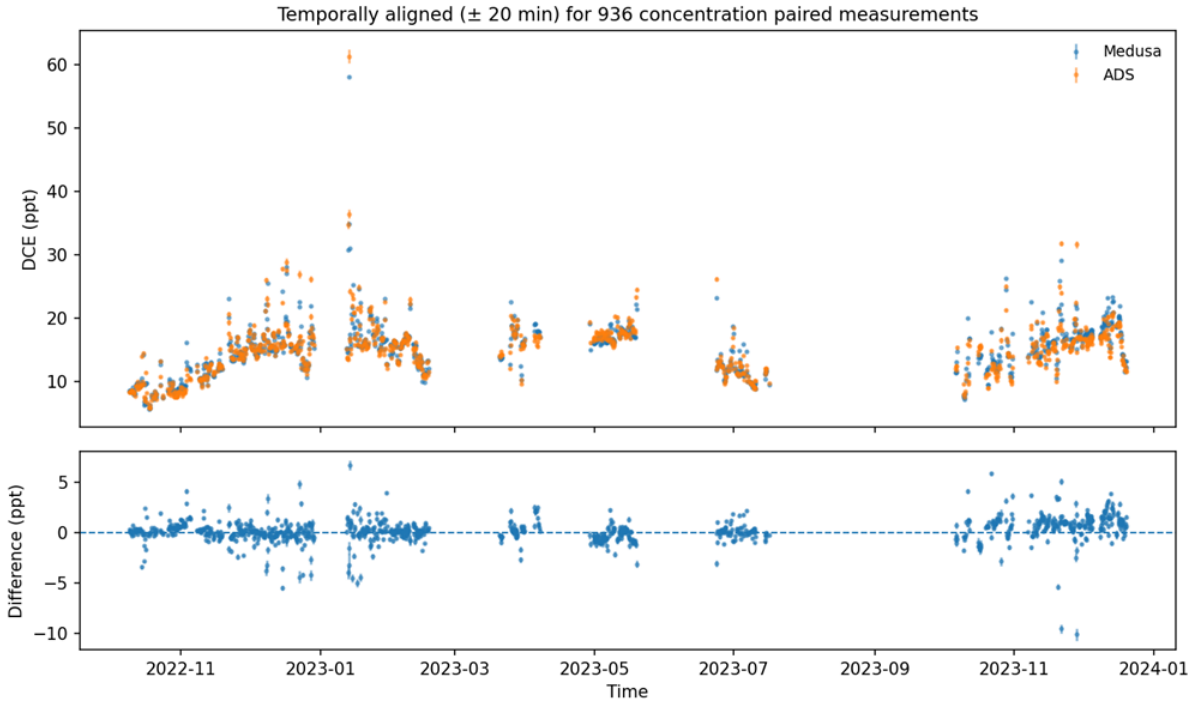

Figure D1. In situ observations of 1,2-dichloroethane (DCE) at Monte Cimone (CMN), Italy, while running two instruments, a Medusa/GC-MS and an Adsorption Desorption System (ADS), in parallel. Temporally matched (± 20 min) measurements are shown, as well as the mole fraction difference between the measurements of the two instruments.

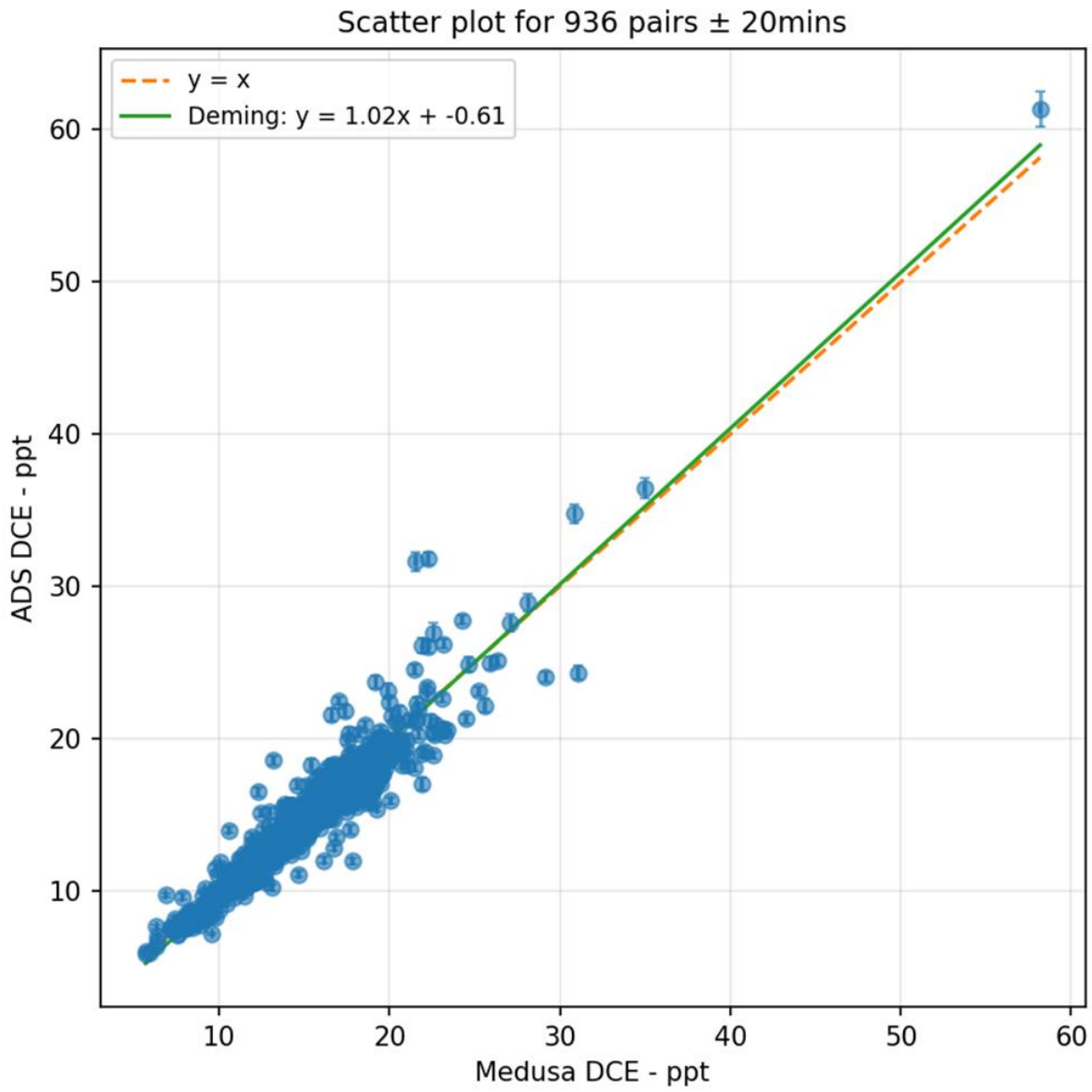

Figure D2. Orthogonal (Deming) regression scatter plot of the temporally matched (± 20 min) in situ measurements of 1,2-dichloroethane (DCE) at Monte Cimone (CMN), Italy, while running two instruments, a Medusa/GC-MS and an Adsorption Desorption System (ADS), in parallel.

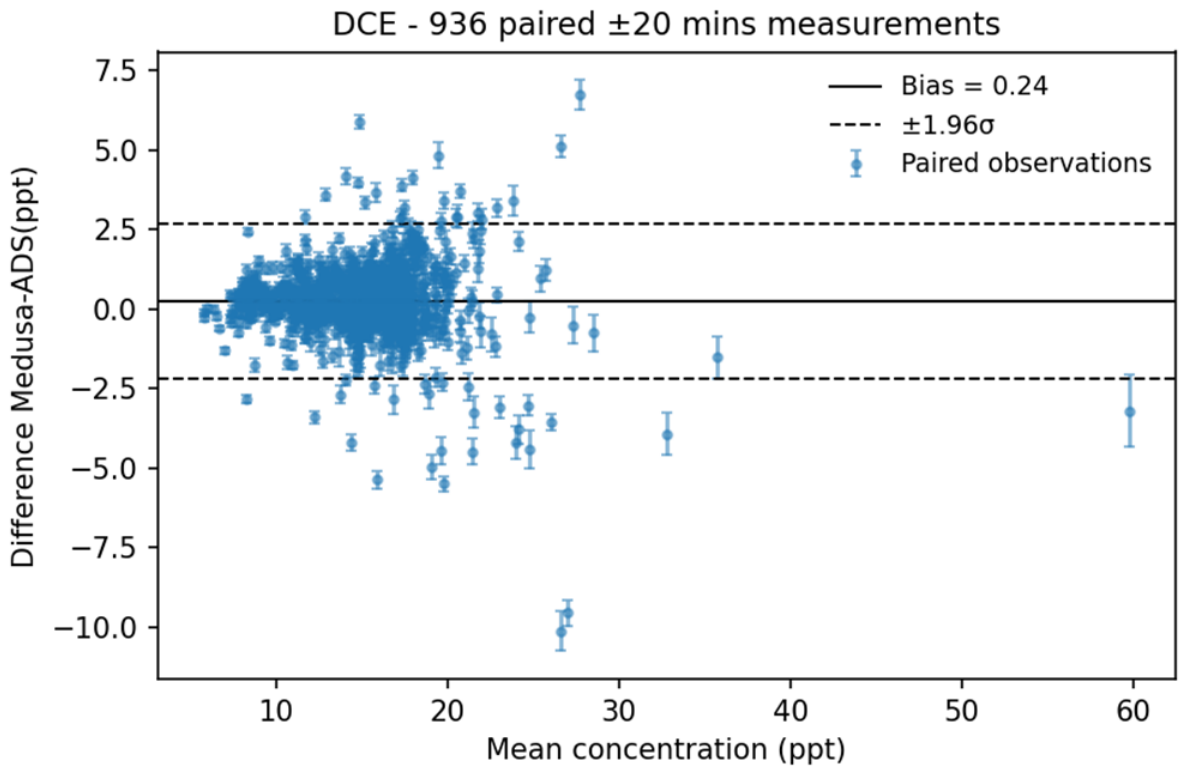

Figure D3. Blant-Alman plot showing the difference between temporally matched (± 20 min) 1,2-dichloroethane (DCE) measurements using the Monte Cimone (CMN) Medusa/GC-MS and Adsorption Desorption System (ADS), as a function of concentration (mole fraction).

Table D1. Statistics for the comparison between temporally matched (± 20 min) 1,2-dichloroethane (DCE) measurements using the Monte Cimone (CMN) Medusa/GC-MS and Adsorption Desorption System (ADS).

Statistic	Value
Number of points	936
Bias	0.24 ppt
RMSE	1.27 ppt
MAE	0.82 ppt
Pearson r	0.954
Spearman rho	0.949

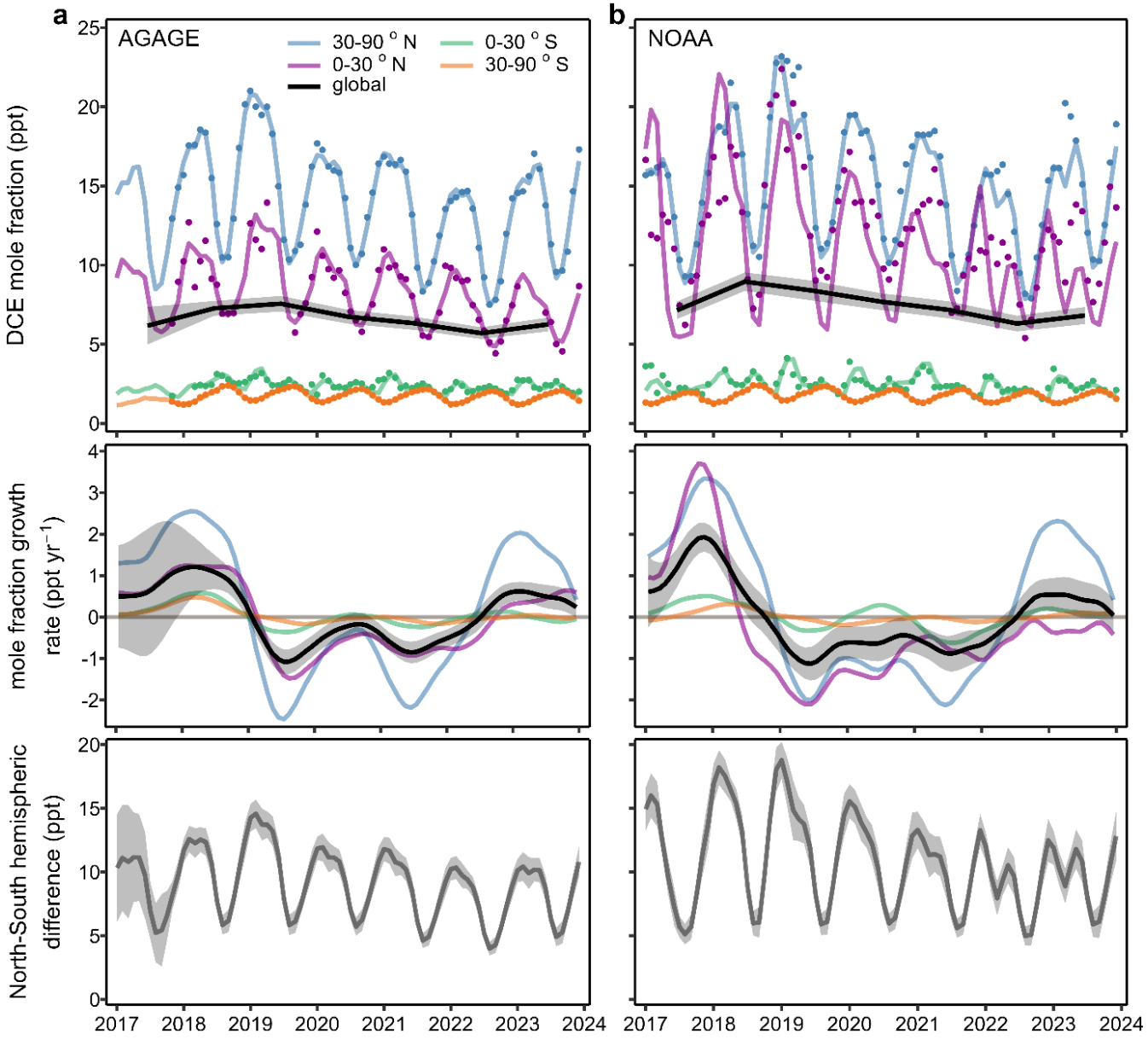

Figure E1. Top row: average global and semi-hemispheric dry-air mole fractions of 1,2-dichloroethane (DCE) derived from measurements from the AGAGE (a) and NOAA (b) networks. The posterior mole fractions from the inversion are shown as lines, with the monthly-mean measured mole fractions shown as markers. Middle row: global and semi-hemispheric mole fraction growth rates. Bottom row: North-South hemispheric mole fraction difference. Uncertainties (grey shaded bands) are given at 1-sigma confidence level.

Table E1. Global annual emissions of 1,2-dichloroethane (DCE) derived from measurements from the AGAGE and NOAA networks, using the AGAGE 12-box model (Western et al., 2025). Uncertainties of the global emissions are given at 1 sigma confidence level.

Year	AGAGE-based global emissions (Gg)	NOAA-based global emissions (Gg)
2017	439 ± 170	509 ± 195
2018	523 ± 196	666 ± 238
2019	508 ± 208	561 ± 231
2020	462 ± 191	529 ± 215
2021	420 ± 182	502 ± 205
2022	385 ± 166	436 ± 184
2023	434 ± 179	474 ± 194

The results of the 12-box model run using the archive data from both networks are shown in Fig. E2, along with the sc05 emissions presented by Hossaini et al. (2024), which were used as the prior mean. Figure E2(a) shows the posterior emission timeseries with the shading representing the full posterior uncertainty arising from both the random and systematic error. This uncertainty is dominated by the systematic component related to the uncertain lifetime of DCE, so it is not noticeably impacted by the sparse data coverage before 2017. Figure E2(b) shows the growth rate in emissions, with the shading representing only the random component of the posterior uncertainty, as the systematic lifetime uncertainty only impacts the absolute emission magnitude and not the emission growth rate. Here the impact of the data sparsity prior to 2017 is clear.

Figure E2(a) shows that the box model posterior emissions are consistent with Hossaini et al. (2024) throughout the timeseries within the 1-sigma uncertainty range of the box model. The central estimate of the box model shows a larger increase in emissions between 2002–2009 compared to Hossaini et al. (2024), but Fig. E2(b) shows that the uncertainty on the box model trend during this period is very large (due to the sparse data coverage) and easily encompasses the growth rate of Hossaini et al. (2024).

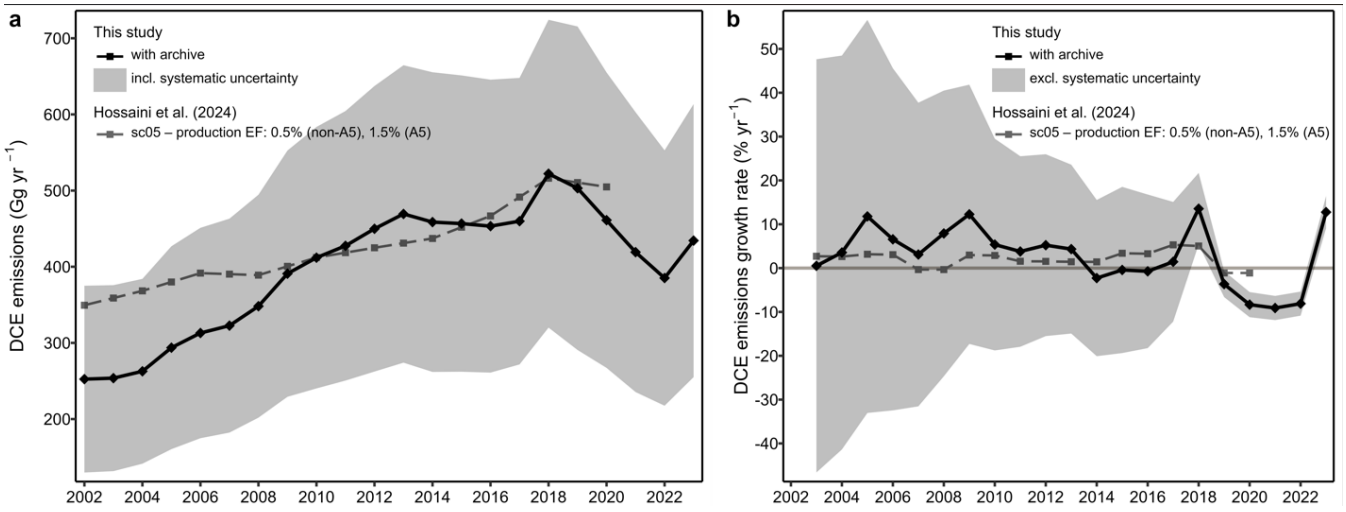

Figure E2. Global emissions (a) and emission growth rate (b) of DCE from the 12-box model, derived using the AGAGE and NOAA archive measurements as well as the AGAGE in situ data post-2017. Also shown are the sc05 emissions derived by Hossaini et al. (2024), which were used as the prior mean. The growth rate for a given year is calculated as the difference between the emissions in that year and the emissions in the previous year.

Appendix F: Additional inverse modelling information and results

Table F1. Details of the differences in model configuration for the four inverse modelling approaches.

	RHIME	InTEM	ELRIS	FLEXINVERT
Bayesian inversion type	Numerical (hierarchical using Markov chain Monte Carlo)	Analytical	Analytical	Numerical (iterative M1QN3 solver)
Dispersion model	NAME	NAME	NAME	FLEXPART
Dispersion model transport duration	30 days	30 days	30 days	10 days
Time step (observation averaging period)	4 hours	4 hours	4 hours	3 hours
Prior background	MHD clean sector (Europe) 12-box model (California)	Manning et al. (2021), adjusted using the annual average RPB:MHD ratio	REBS method based on MHD observations	REBS method based on individual sites

Figure F1 shows the prior and posterior 1,2-dichloroethane (DCE) emission time series for both regional domains. These are the same posterior data shown in Fig. 6, but in this plot the prior has been added for comparison. In both cases the large reduction in posterior emissions (relative to the prior) is clearly evident. Figure F2 shows the prior spatial distribution on two different linear colour scales and the posterior spatial distribution on a linear colour scale (i.e. these are the linear equivalents of Fig. 7).

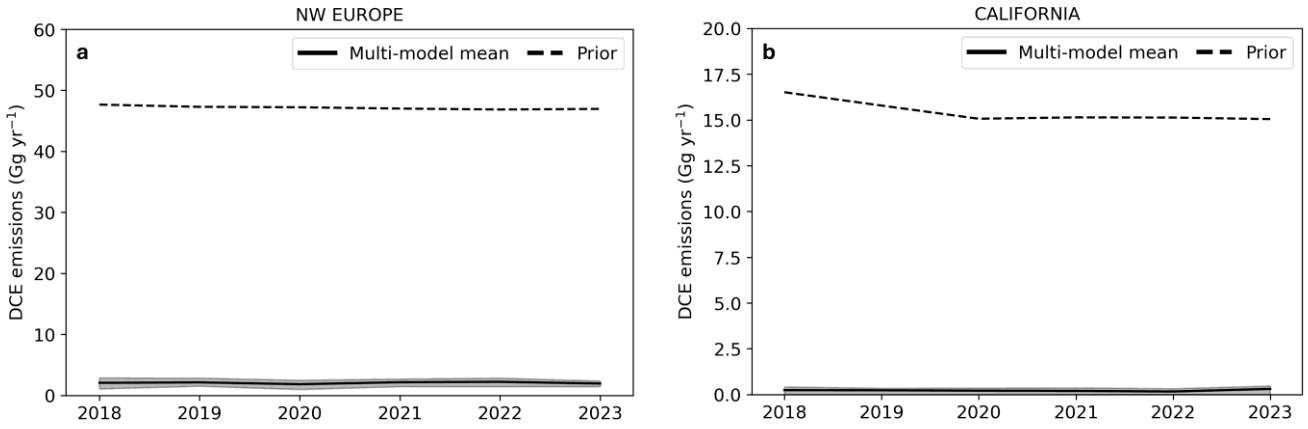

Figure F1. Time series of prior and posterior (multi-model mean) 1,2-dichloroethane (DCE) emissions for NW Europe (a) and California (b). The grey shading represents the range between the lowest 15.9 percentile and the highest 84.1 percentile for any of the individual models.

A sensitivity test for the NW Europe inversions was run using a uniform land prior totalling 4.2 Gg yr^{-1} over the NW Europe region (with the same emission per unit area for applied for all land areas within the domain). The posterior time series for all four models using both priors are shown in Fig. F3(a). Posterior time series showing individual model uncertainties are also shown for the California region in Fig. F3(b). Even though the prior emissions total for NW Europe differs by an order of magnitude between the two priors, the total posterior emissions for NW Europe are relatively insensitive to the choice of prior.

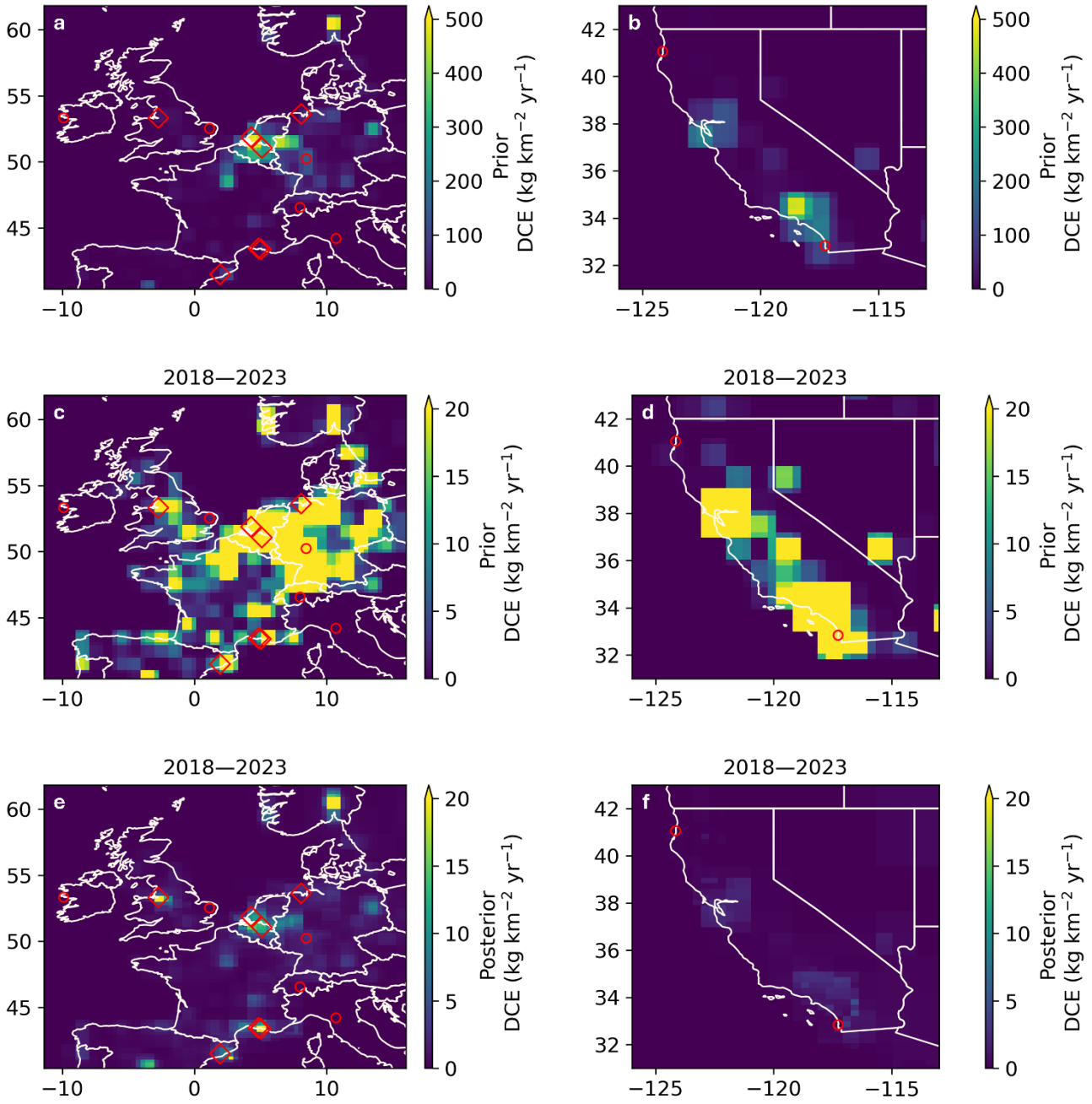

Figure F2. Prior (a–d) and posterior (e, f) 1,2-dichloroethane (DCE) emissions for NW Europe (a, c, e) and California (b, d, f). The red circles denote the measurement sites, and the red diamonds show the locations of facilities known to be large producers and/or users of DCE. The same prior data is shown on a wider colour scale (a, b) and a highly saturated colour scale (c, d) for better comparison against the posterior (e, f).

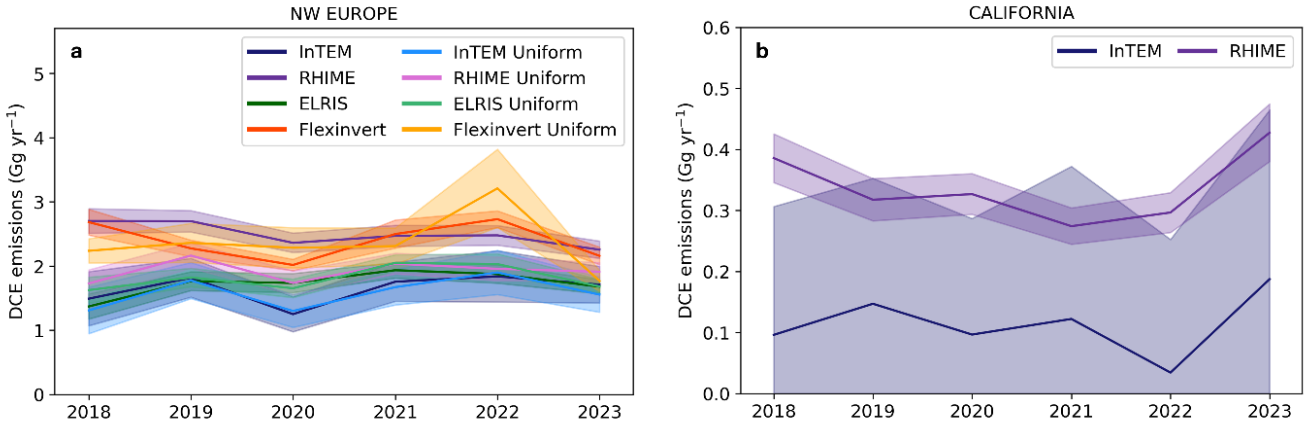

Figure F3. Posterior time series of DCE emissions with each model run (and its associated uncertainty) shown separately for northwest (NW) Europe (a) and California (b). For NW Europe both the base case Hossaini et al. (2024) prior and a uniform prior with the same emission per unit area distributed over all land areas (with the total equal to 4.2 Gg yr^{-1} over NW Europe) are shown.

The posterior spatial distributions for NW Europe are shown separately by model and prior in Fig. F4. In general, the models have a similar spatial distribution of posterior emissions in the NW Europe countries for which we have high sensitivity (Belgium, Germany, France, UK, Ireland, Luxembourg and the Netherlands), regardless of the prior used. The posterior spatial distribution for FLEXINVERT exhibits a greater dependency on the prior relative to the other models, while the impact of the prior on total posterior emissions for NW Europe (Fig. F3) is largest for RHIME.

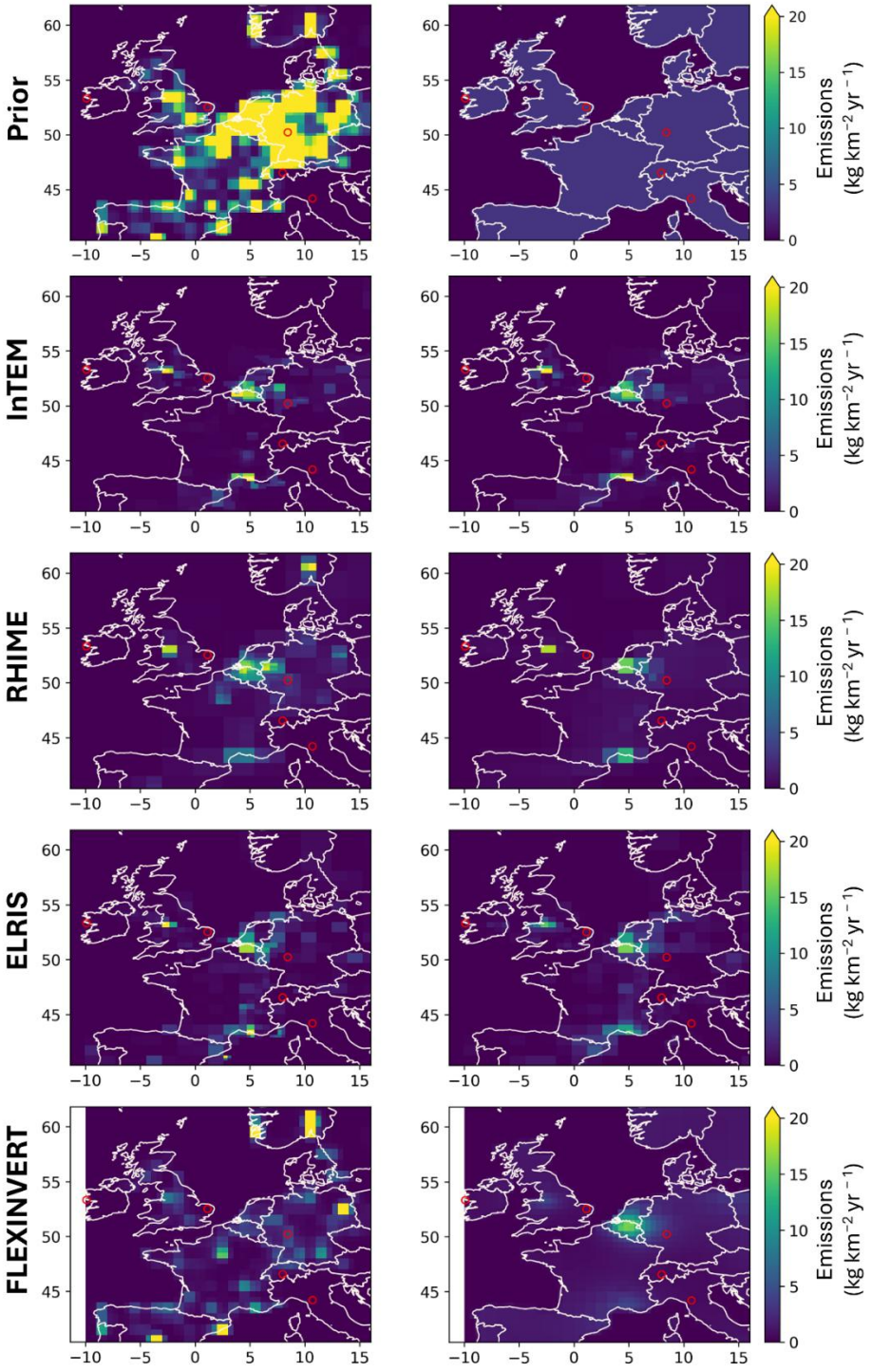

Figure F4. Prior (top row) and posterior (bottom four rows) emissions from all four models using both the base case prior (left column) and the uniform land prior (right column).

Appendix G: PRTR emissions

Table G1. Annual emissions for NW Europe from the combined European Pollutant Release and Transfer Register (E-PRTR) (EEA, 2026) and UK-PRTR (DEFRA, 2012).

Year	NW Europe emissions (Gg)
2018	0.82
2019	0.76
2020	0.98
2021	0.80
2022	0.72
2023	0.62